NUREG/CR-0790
SAND79-0909
R7

TOPICAL REPORT ON FUEL MOTION DIAGNOSTIC SYSTEMS

S. A. Wright, Editor

Printed October 1979

Sandia Laboratories

Prepared for

U. S. NUCLEAR REGULATORY COMMISSION

Available from
National Technical Information Service
Springfield, VA 22161

NUREG/CR-0790
SAND79-0909
R7

TOPICAL REPORT ON FUEL MOTION DIAGNOSTIC SYSTEMS

S. A. Wright, Editor

Date Published: October 1979

Sandia Laboratories
Albuquerque, New Mexico 87185
operated by
Sandia Corporation
for the
U. S. Department of Energy

Prepared for
Division of Reactor Safety Research
Office of Nuclear Regulatory Research
U. S. Nuclear Regulatory Commission
Washington, D. C. 20555
Under Interagency Agreement DOE 40-550-75
NRC FIN No. A-1016

SPECIALIST MEETING ON FUEL AND CLAD
MOTION DIAGNOSTICS FOR FAST REACTOR
SAFETY TEST FACILITIES
DECEMBER 5 - 7, 1977

CONTENTS

ILLUSTRATIONS

INTRODUCTION

The Specialist Meeting on Fuel and Clad Motion Diagnostics for Fast Reactor Safety Test Facilities took place on 5-7 December 1977 in Los Alamos, New Mexico. The meeting was sponsored by the U. S. Nuclear Regulatory Commission (NRC), the U.S. Department of Energy (DOE) and the Organization for Economic Cooperation and Development to facilitate the exchange of technical information on the latest developments in diagnostic techniques and to help define the necessary fuel motion diagnostic requirements for future safety test facilities.

Representatives from LASL, ANL, and Sandia attended as did representatives from Oregon State University, the University of Washington and the CABRI project.

This report contains only the papers contributed by Sandia. Because the notification date of this meeting was late, many of the contributions were in abstract form. Since the meeting, the authors have updated their written contributions to include the information presented orally at the meeting. The papers contained in this report, therefore represent the accomplishments as of December 1977.

The first three papers address the topic of coded aperture imaging. The first paper describes two experiments showing that fuel pins illuminated by reactor radiation can be observed and that collimators can be designed to give more-than-adequate signal-to-background ratios. The second paper discusses the methods of analog and digital reconstruction of pseudoholograms. The third paper treats imaging in large fuel pin bundles. Both gamma radiation and fast neutrons are considered as imaging sources.

The final two papers deal with alternative techniques for monitoring fuel motion by addressing in-core fuel motion detection and flash x-radiography. The paper on in-core fuel motion detection describes the mathematical relationship between detector response and fuel motion. The paper on flash x-radiography defines the x-ray source required and describes experiments which illustrate the problems of imaging fuel motion under conditions of poor geometry.

CHAPTER 1

THE DEVELOPMENT OF A CODED APERTURE FUEL MOTION DIAGNOSTICS SYSTEM FOR THE ACPR (UPGRADE)

J. G. Kelly and K. T. Stalker
Sandia Laboratories, Albuquerque, New Mexico

As part of Sandia Laboratories' program to study simulated core disruptive accidents in reactor safety research, a fuel motion detection system based on coded aperture imaging[1,2] is being developed for the Annular Core Pulsed Reactor (ACPR).[3,4,5] Although fuel motion has been observed at the TREAT by the fast neutron hodoscope[6] and with a Vidicon pinhole camera technique,[7] the coded aperture system offers a potential for lower cost, higher spatial resolution, three dimensional imaging, and higher frame rates at lower fluences than either of the other techniques. At earlier conferences the imaging of fuel pin shaped fission γ-ray sources has been reported, but until the experiments which will be reported here were conducted, it was not known whether either of two important questions could be properly answered. First, could a fuel pin illuminated by a reactor be imaged with a coded aperture and an active detector system with acceptable frame rates and spatial resolution? Second, could collimator and shield structures be fabricated for the ACPR to provide acceptable signal-to-background ratios?

Both of these questions can now be answered in the affirmative because of the favorable experiments recently conducted at the Sandia Pulsed Reactor (SPR-II) and at the ACPR. The techniques used for the reconstruction of images will be presented in the next paper.[8]

Before these feasibility tests are discussed in detail, a review of the coded aperture imaging technique will be given. This review will be brief because the principles have been presented in the literature.[1,2]

The main advantages for imaging a coded aperture is over a pinhole aperture is that it can collect photons and locate their spatial origin at a much higher rate. In addition, 3-dimensional information can also be obtained. Figure 1.1 shows how this is accomplished with a Fresnel zone plate. The γ-ray fluxes from two positions on the object are illustrated. For each, a Fresnel shadow pattern is impressed onto the detector. The lateral position of the object point determines the lateral position of the image point. Also depth information is recorded because the size of the rings in the zone plate pattern is determined by the relative spacings between the object point, the

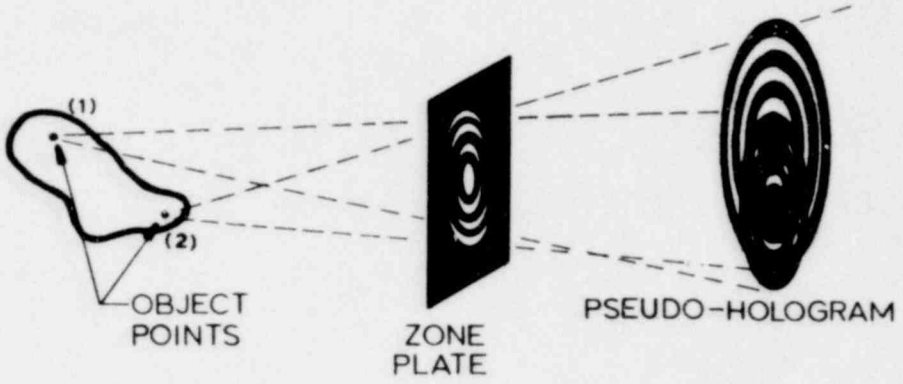

· PSEUDO-HOLOGRAM FORMATION FROM TWO OBJECT POINTS

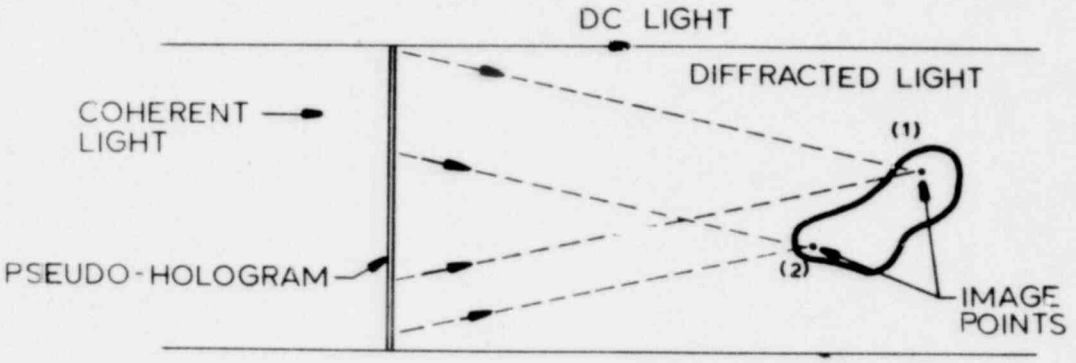

Figure 1.1. Method of Obtaining 3-Dimensional Information Using a Fresnel Zone Plate.

aperture and the detector plane (S_1 and S_2). The pseudohologram of any object is therefore composed of a linear superposition of elementary scaled Fresnel patterns.

If now a coherent laser beam is directed through a transparency of the pseudohologram, each elementary zone plate pattern will act as a diffraction lens. At some distance behind the film plane all of the wavelets passing through the transmitting zones will be in phase at the center of this elementary pattern. A bright spot will therefore appear at that position. The spatial distribution of these focused points traces out the image. Superimposed on this image is an additional background made up of undiffracted light passing through the pseudohologram and light from other out-of-focus object points. A major portion of the research in coded aperture imaging has been devoted to understanding, quantifying and reducing these backgrounds.

The significant feature of this method is that by this two step process a γ-ray lens has effectively been created.

The code that has been primarily used for fuel rod studies at Sandia Laboratories is shown in Figure 1.2. As in a Fresnel plate, the radii of the zones are given by $r_n = r_1\sqrt{n}$, but for long thin objects the signal-to-noise ratio in the image is much better with this linear code. It has the same radial resolution as a 1 mm wide pinhole but collects photons at 20 times the rate. The linear aperture made of Ta vanes was used in both of the major feasibility tests that will now be discussed.

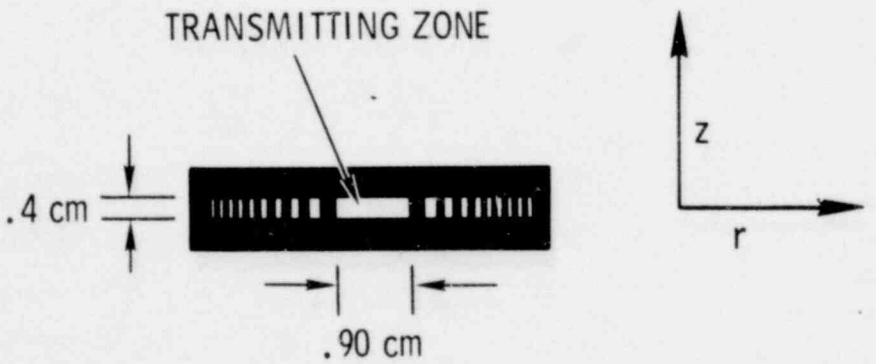

Figure 1.2. Code Used for Fuel Rod Studies.

The SPR-II Active Imaging Experiment was conducted to verify that a fuel pin illuminated by neutrons could be imaged in the presence of a reactor with an active detector system. The SPR-II is a short pulse, fast reactor of the Godiva type.[9] The neutron burst lasts from 50 to 200 μsec depending on whether moderating material is in the vicinity. The 200 μsec burst period corresponds approximately to the minimum frame period of the fuel motion system. Rough estimates also indicated that the signal intensity from the pin would be close to that expected during one 200 μsec frame period during the peak of a moderate ACPR burst. Thus the test would be a good measure of system signal-to-background ratio, gain and resolution.

Beside the reactor core, 20 percent enriched and 93 percent enriched fuel pins were positioned as shown in Figure 1.3 and were observed by a coded aperture and collimator mounted in the reactor shield wall. The detectors were x-ray films and two types of active recording systems. The first was an x-ray image intensifier optically coupled to a still camera or to a framing camera. The second was a thin NaI scintillator plate observed with an optical image intensifier and cameras. Although the fuel pin pseudohologram was visible in all three detector arrangements, only the x-ray film and the x-ray intensifier provided reconstructable holograms. The spatial resolution provided by the NaI proved to be too poor. Investigations at Los Alamos have indicated that a commercial x-ray intensifier screen, Quanta II, has more sensitivity and better spatial resolution than an equal thickness NaI.[10] This and other screens will also be tested for application in this fuel motion detection system.

A pseudohologram recorded on 35 mm film in the camera behind the x-ray intensifier was inserted directly into the laser reconstruction system and was also digitized for computer reconstruction. Both types of reconstructions will be discussed in the next paper (Chapter 2). Suffice it to say at this point that the fuel pin images are readily discernable above background.

The exposures obtained however were of lower intensity and had a poorer signal-to-noise ratio than had been expected. Subsequent investigation revealed that the polyethylene blocks placed on each side of the pin to thermalize neutrons were actually borated, and the neutron fluence was 20 times smaller than projected. The fact that acceptable images were obtained indicates that the coded aperture technique with active recording is very sensitive and will indeed be very

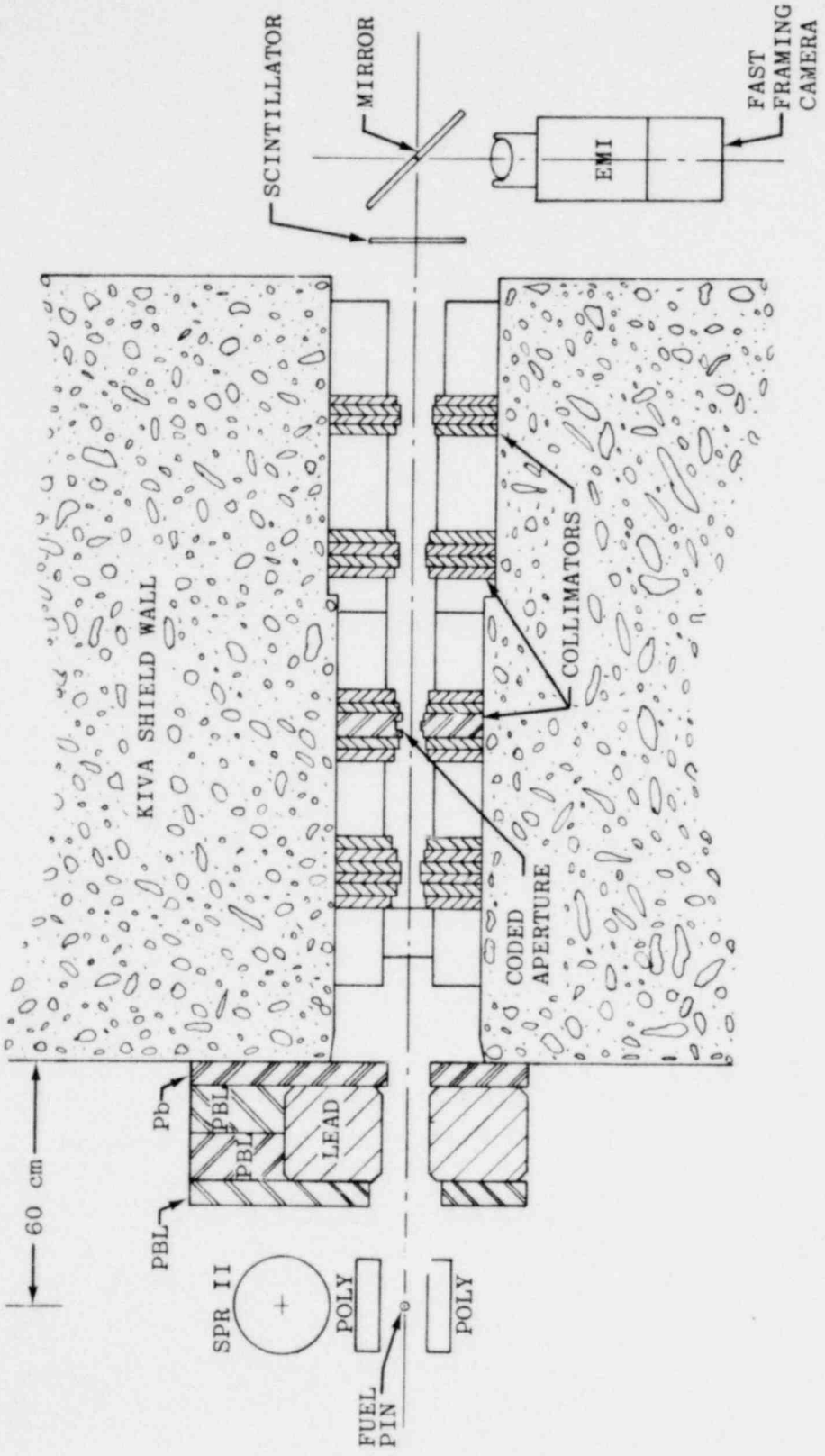

Figure 1.3. SPR-II Fuel Pin Imaging Geometry.

useful in the fuel motion application. This will be the case if an acceptable signal-to-noise ratio can be obtained at ACPR.

The Collimation Test Module (CTM) Experiment at ACPR was designed to determine whether the signal from a fuel pin placed in the central test chamber could be seen above background. The answer was yes. ACPR fuel rods were removed to form a slot through which a fuel pin in the central test chamber could be viewed by the coded aperture and a double tapered collimator that penetrated the external shield. A sketch of this module is shown in Figure 1.4. This shield structure was very limited in thickness and size because it had to be compatible with the neutron radiography tube present in the reactor tank. There was also no room for an active detector system in the very small detector region available at that time. X-ray film was therefore used as a detector and the reactor was operated at a low level steady-state mode to prevent the test fuel pin from being damaged by fission heating. The UO_2 pellets in the pin were 0.5 cm in diameter and enriched to 20%. They were encased in a close-fitting, stainless-steel tube with a 0.22 cm thick wall. A fluted molybdenum spacer tube then centered in the pin in a 1.52 cm O.D. by 1.27 cm I.D. inconel containment casing. The whole assembly was held in a canister designed for prompt burst excursion experiments. Except along the slot line of sight, the canister was lined with 3.1 cm of polyethylene for neutron thermalization, and behind the pin a block of 3.8 cm thick lead attenuated the scene background from the reactor wall. A lead collimator penetrated the core where the removal of fuel rods had left a gap about two rows wide. Outside the core, layers of steel, a solution of $NaBF_4$ and lead provided the bulk shielding. The view through the collimator is illustrated in Figure 1.5

Within and around the film chamber, a rather extensive set of dosimetry and film measurements was made to characterize the radiation environment at the detector. During a steady-state run in which 100 MW sec was generated in the reactor and about 500 cal/gram deposited in the fuel pin, it was found that the radiation field at the film plane consisted of a number of different components. There was a very low energy photon component which exposed the film but which caused almost no response in the thermoluminescent (TLD) dosimeters. This background can be almost entirely eliminated if 0.125 mm of Ta is placed on each side of the film. The Ta also acts as an intensifier by increasing the effective sensitivity of the film to the higher energy photon field by a factor of 2. There was a diffuse hard γ-ray background of about 11 rads coming through the collimator. Superimposed

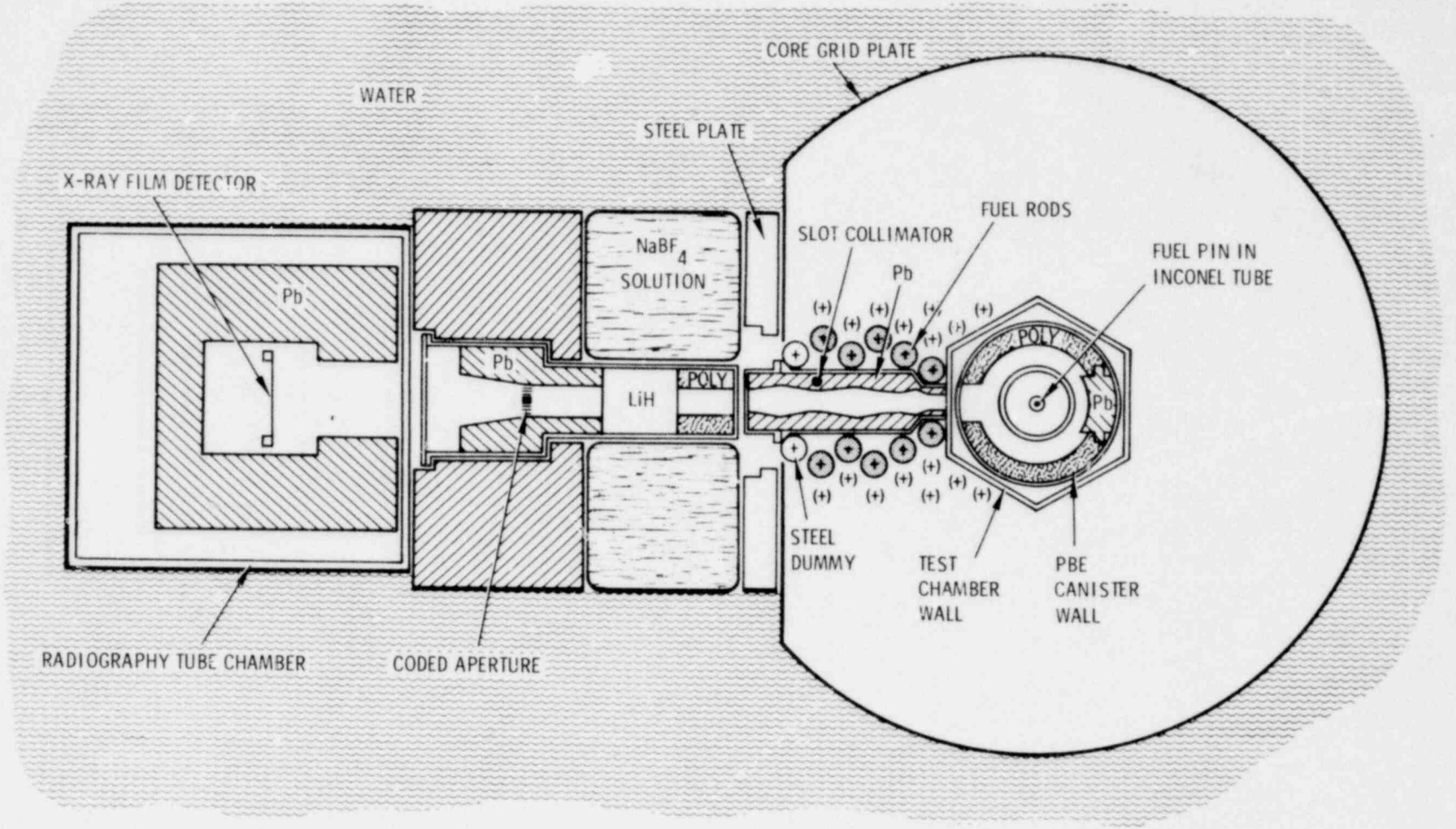

Figure 1.4. Collimation Test Module.

on these backgrounds (when the fuel pin was in place) was a signal of about 1.5 rads. The latter two of these higher energy components can be seen in the film-recorded pseudoholograms that are shown in Figure 1.6. The two pictures are contact prints of the original x-ray film exposure in which the diffuse background has been cut out below the toe of the contact print film response. The dark band at the top is from γ-ray scattering in the steel flange sketched in Figure 1.5. The additional structure present when the fuel pin is in place is clearly visible in Figure 1.6b.

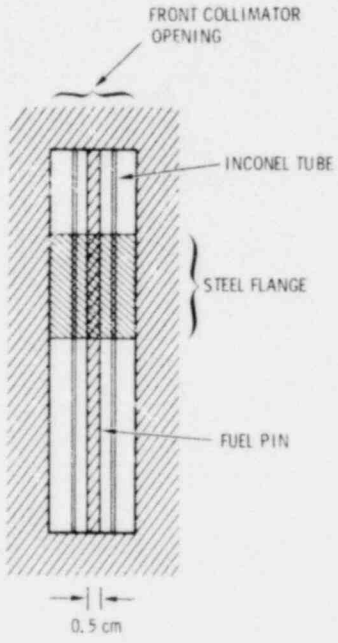

Figure 1.5. View Through the Collimator.

The densitometer traces taken across the x-ray films are shown in Figure 1.7. The two lower scans were taken above the collimated beam and show the chamber background, while the upper scans include the signal, scene background and the chamber background contributions. The signal from the pin contributes only about 7% of the total exposure. This may seem marginal, but this is just the kind of circumstance in

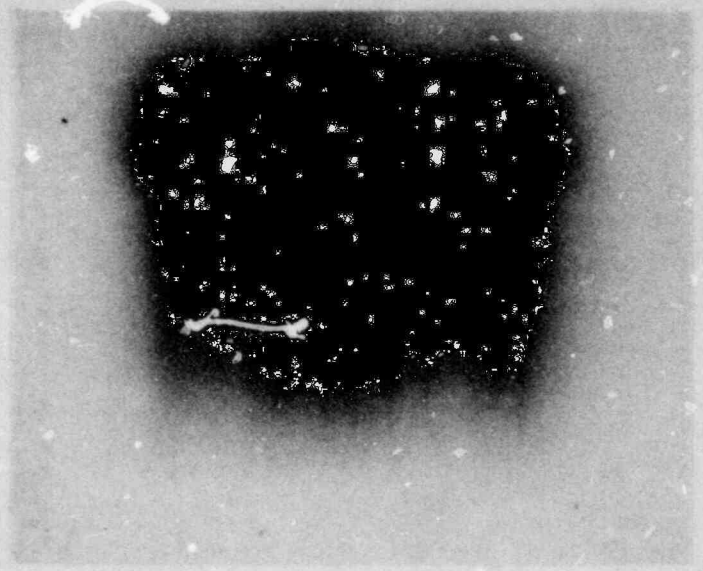

(A) SHADOWGRAM OF VIEW THROUGH THE CODED APERTURE INTO THE PBE CANISTER WITH NO FUEL PIN

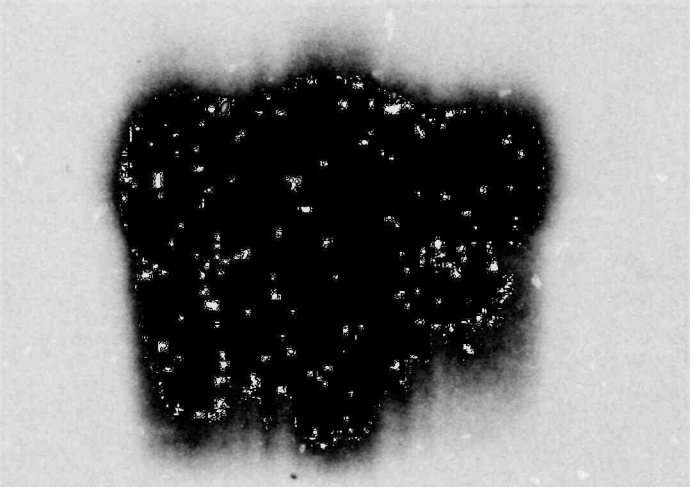

(B) SHADOWGRAM OF VIEW THROUGH THE CODED APERTURE INTO THE PBE CANISTER WITH A FUEL PIN

Figure 1.6. Film-Recorded Pseudoholograms.

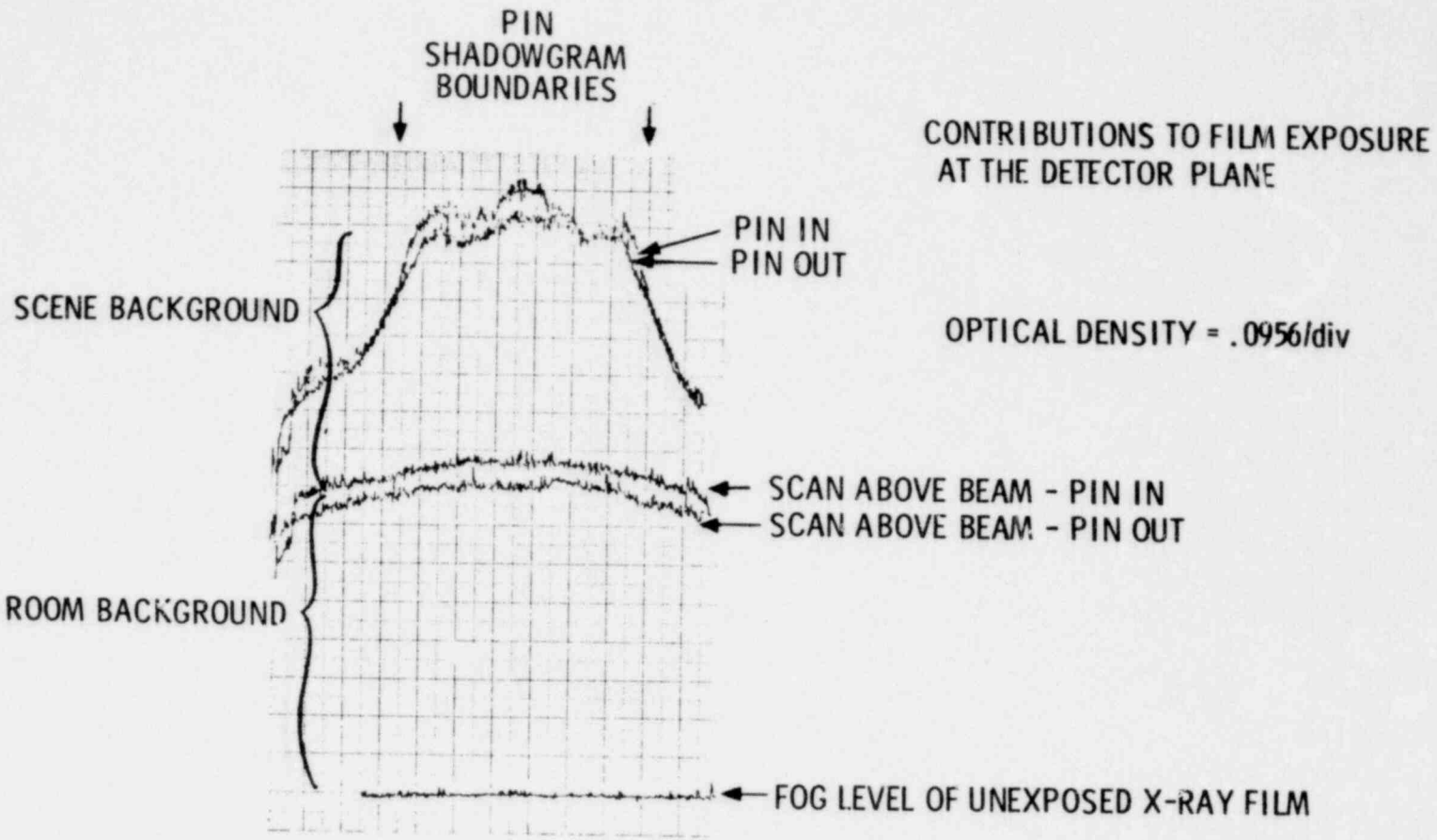

Figure 1.7. Densitometer Traces Taken Across the X-Ray Films.

which the advantages of coded aperture imaging exhibit themselves most effectively. The reconstructed images which will be discussed in the next paper[8] indicate that from this type of data a signal-to-background ratio in the final image may be as high as 10 to 1.

Some conclusions which are relevant for the final system can be made on the basis of this experiment and are listed below:

1) Sheets of Ta pressed against the film act very effectively both as low energy filters and as signal intensifiers.

2) A quality pseudohologram can be obtained on type AA x-ray film in 4 minutes at 10 kW reactor power. This is approximately the same exposure as would take place during a 500 cal/gram ACPR pulse in a 200 μsec time period. This is without any signal amplification.

3) The lead shield behind the pin provides a significant reduction in scene background.

4) Analysis has indicated that most of the chamber background is produced by inelastic scattering of neutrons near the rear surface of the lead shield. The background should be significantly reduced by the addition of more water or polyethylene ahead of the lead shield.

5) A coded aperture with higher modulation in the finer zones will be much more effective. An improved aperture is being made for the final system.

The principal conclusion that can be drawn from this experiment is that the required information about the fuel pin can be made available outside the slot in the reactor core. In addition there are many straightforward improvements which will be made in the final system that will significantly improve the pseudohologram structure at the detector plane. The primary remaining task is to properly engineer the total fuel motion Coded Aperture Imaging System (now known as CAIS) for optimum performance.

References

1. H. H. Barrett and F. A. Horrigan, Appl. Opt., 24, 2686 (1973).
2. H. H. Barrett, W. W. Stoner, D. T. Wilson, and G. D. DeMeester, Optical Eng. 13, 539 (1974).
3. J. G. Kelly and D. A. McArthur, Trans. Amer. Nucl. Soc., TANSAO 22 395 (1975).
4. J. G. Kelly and K. T. Stalker, Proc. Int. Conf. on Fast Reactor and Related Physics, Chicago (1976). (In Print).
5. K. T. Stalker and J. G. Kelly, Proc. SPIE/SPSE Tech. Symp. on X-Ray Imaging, 106-11, April (1977).
6. A. DeVolpi, R. J. Pecina, R. T. Daly, D. J. Travis, R. R. Stewart, and E. A. Rhodes, Nucl. Tech. 27, 449 (1975).
7. G. J. Berzins and K. S. Han, Nucl. Sci., and Eng., to be published (1977).
8. K. T. Stalker and J. G. Kelly, Contribution to the 3rd Annual Conference on Fuel and Clad Motion Diagnostics, Los Alamos Scientific Laboratory, 1977.
9. J. A. Snyder, SPR-IIA Experimenter's Manual, SC-M-69-289 Sandia Laboratories, May 1969.
10. W. Stein, private communication.

CHAPTER 2

ANALOG AND DIGITAL RECONSTRUCTIONS OF FUEL PIN IMAGES RECORDED WITH THE PROTOTYPE ACPR (UPGRADE) FUEL MOTION DIAGNOSTIC SYSTEM

K. T. Stalker and J. G. Kelly
Sandia Laboratories, Albuquerque, New Mexico

A coded aperture imaging system to provide time resolved images of LMFBR fuel rods undergoing simualted core disruptive accidents is being developed at Sandia Laboratories.[1,2] The previous paper (Chapter 1) described two experiments performed at the Sandia Pulsed Reactor (SPR-II) and the Annular Core Pulsed Reactor (ACPR). The results of these experiments demonstrated the feasibility of time resolved coded aperture imaging as a diagnostic tool in fuel motion measurement. This Chapter will present the imaging results of the SPR-II and ACPR experiments and will discuss how the information was decoded from the coded image. The results of two different methods of image reconstruction will be presented and the relative merits of both approaches will be discussed.

This discussion will first address an analog optical reconstruction technique the apparatus for which is sketched in Figure 2.1. In this technique the pseudohologram is placed in a converging beam of light which causes the undiffracted background light to come to focus at a different plane than the image. This allows an opaque beam stop, called a d.c. stop, to increase the contrast in the reconstructed image by blocking the undiffracted background light while allowing the image to be seen at the zone plate focal plane. Reconstructed images of the SPR-II and ACPR experiment are shown in Figures 2.2 and 2.3 respectively.

The reconstructed images from the SPR-II experiment are shown in Figure 2.2. The original pseudohologram was obtained using a 35 mm camera to photograph the output phosphor of the x-ray image intensifier (detector). This pseudohologram was contact printed onto high contrast film to improve its diffraction efficiency and then reconstructed using the system previously described. Figure 2.2a shows the reconstructed image of a single 93% enriched fuel pin within the field of view. Figure 2.2b shows the reconstructed image of two fuel pins, one 93% enriched and the other 20% enriched. The circular rings seen in these reconstructions are caused by diffraction from the circular boundary defined by the 20 mm diameter output phosphor of the x-ray image intensifier. These unwanted fringes can be eliminated by apodizing the

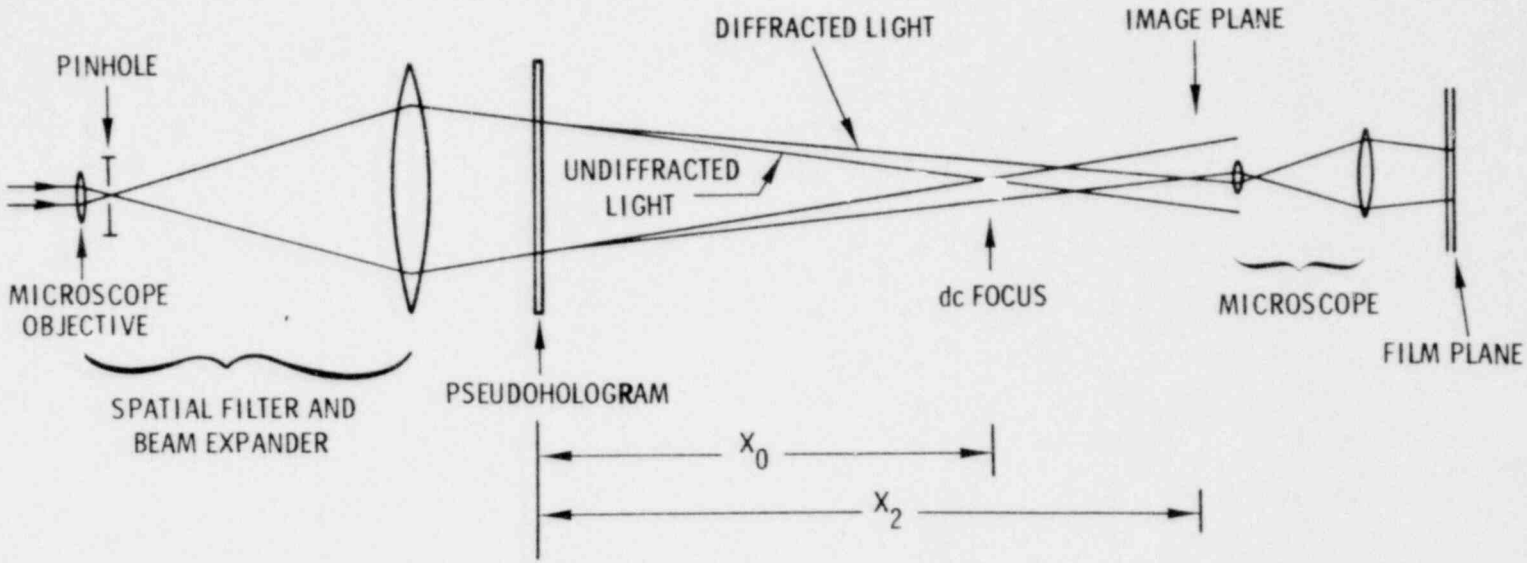

Figure 2.1. Analog Optical Reconstruction System.

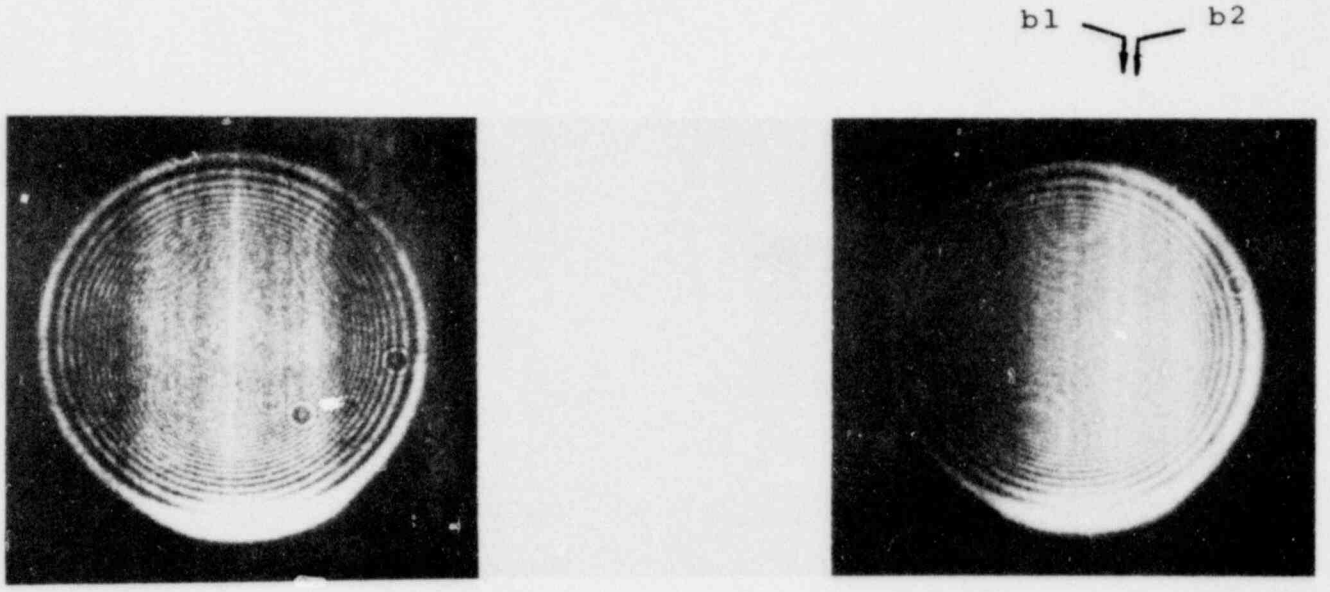

(a) Single Pin

(b) Two Pins

(b1) 93% enriched

(b2) 20% enriched

Figure 2 2. Laser Reconstructions of LMFBR Fuel Pins Illuminated by Neutrons from the Sandia Pulsed Reactor. Recorded with an X-ray Image Intensifier.

boundary region in the original pseudohologram. No d.c. stop was used in this case because it seemed to increase the contrast of the unwanted circular fringes and distract from the reconstructed image.

The reconstructed images from the ACPR experiment are shown in Figure 2.3. In this case the original pseudohologram obtained on radiographic film was photoreduced onto high contrast film and then optically reconstructed. Figure 2.3a shows the reconstructed image of the PBE canister with a fuel pin in place while the PBE canister without the fuel pin is shown in Figure 2.3b.

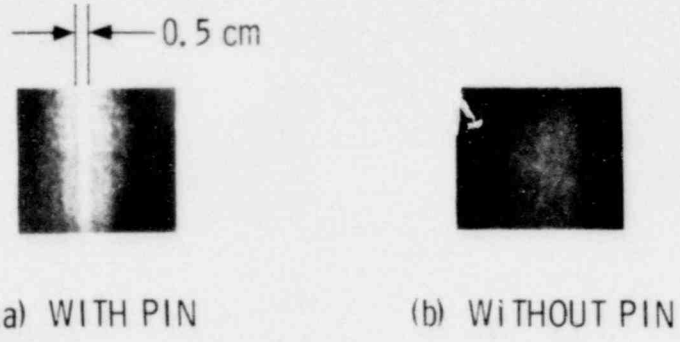

Figure 2.3. Optical Reconstruction of an LMFBR Fuel Pin Illuminated by Neutrons from the Annular Core Pulsed Reactor. Figure 2.3a Shows Fuel Pin Image. Figure 2.3b Shows Experimental Configuration Without the Fuel Pin in Place.

Figure 2.4 (a and b) are densitometer scans taken through a photographic transparency of the "pin in" and "pin out" reconstructions shown in Figure 2.3. Comparing both the actual reconstructions in Figure 2.3 and the scans in Figure 2.4 reveals that there is some signal present even when the fuel pin is not in the PBE canister. The fuel pin reconstructions of Figure 2.3a and the densitometer scan of Figure 2.4a are indicative of a width and edge resolution on the order of 2 mm. Actual resolution numbers could be obtained from the scans only after the careful calibration of the film characteristics involved in all the photographic steps involved. Steps are currently being taken to accomplish this. The "pin in" pictures also show some evidence of two lighter

bands on each side of the pin. These bands are just the right radii to be associated with the edges of the inconel containment tube, but proof is still required that these bands are actually caused by the steel. Some of this structure may be caused by overshoot and oscillation in the image intensity introduced by the d.c. filtering employed to increase image contrast and reduce the undesired broad background illumination. The actual origin of these bands is currently under investigation.

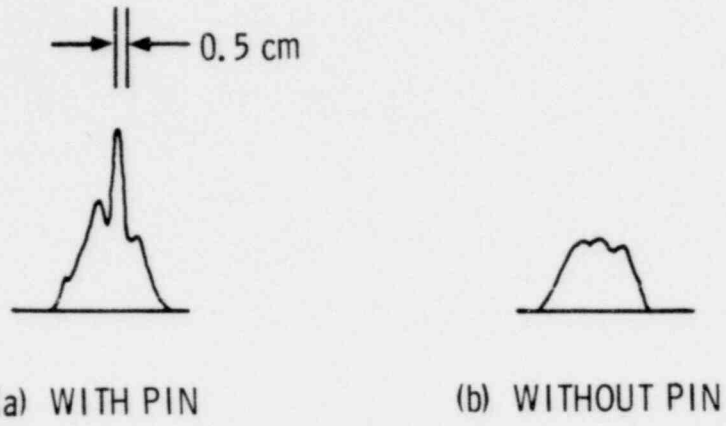

Figure 2.4. Densitometer Scans Through Photographic Transparency of the "Pin-in" and "Pin-out" Image Reconstructions Taken on Polaroid P/N 55 Film.

The second reconstruction technique which can be employed is digital reconstruction. The steps in this process are outlined in Figure 2.5. First the pseudohologram is digitized on a scanning microdensitometer producing a two dimensional array of density values which are then converted from density to input exposure energy using the characteristic curve for the film used. Following this, the average value of each row is calculated and subtracted from each value in the row. At this point several algorithms may be employed to reconstruct the image. The one used to produce the results shown in Figures 2.6 and 2.7 are computer analogs of the Fresnel diffraction process which takes place in the laser reconstruction technique. To implement this technique each array value in a row is multiplied by a quadratic phase factor and then Fast

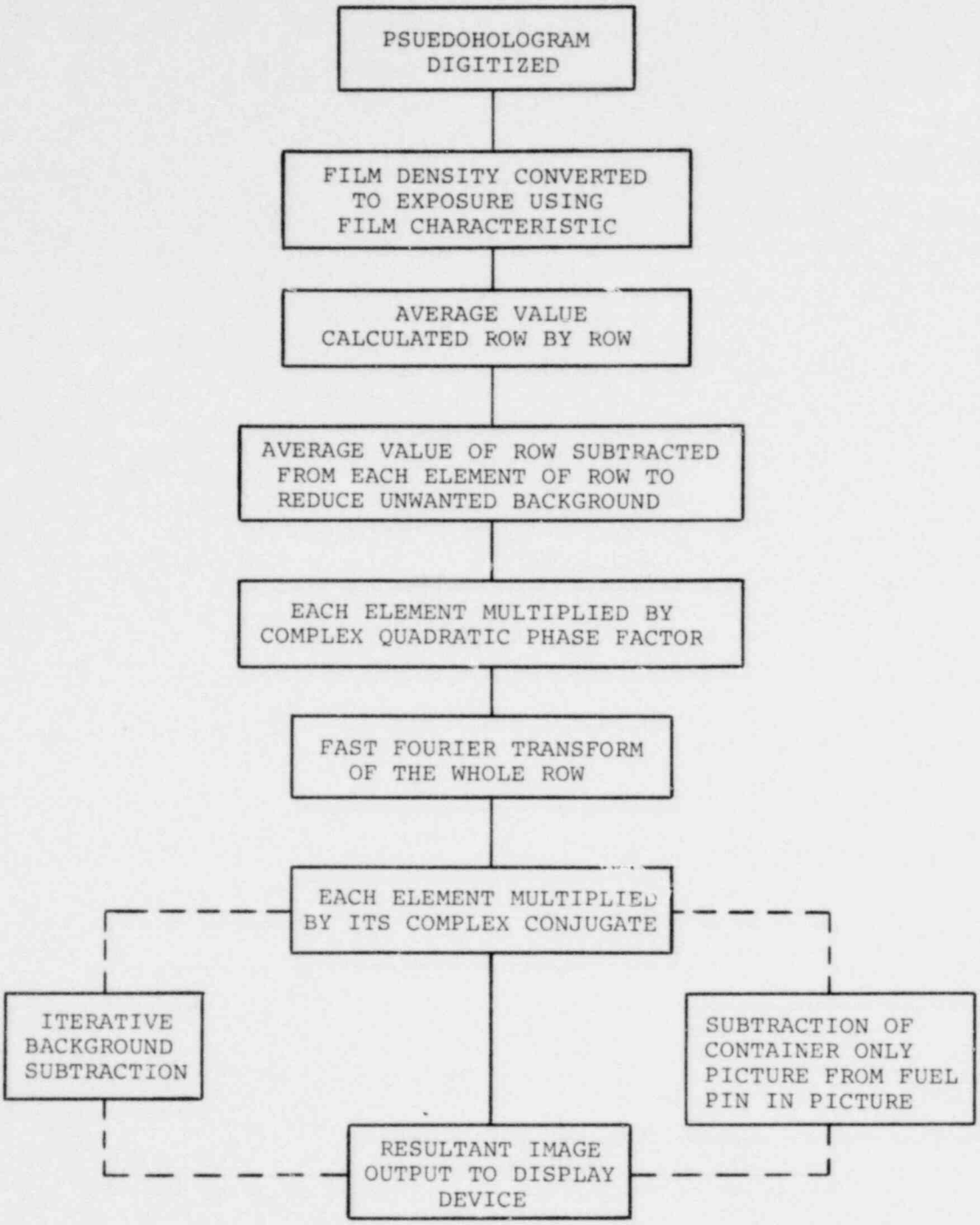

Figure 2.5. Block Diagram of Steps Required on Digital Computer Reconstructions of One Dimensional Coded Aperture Images.

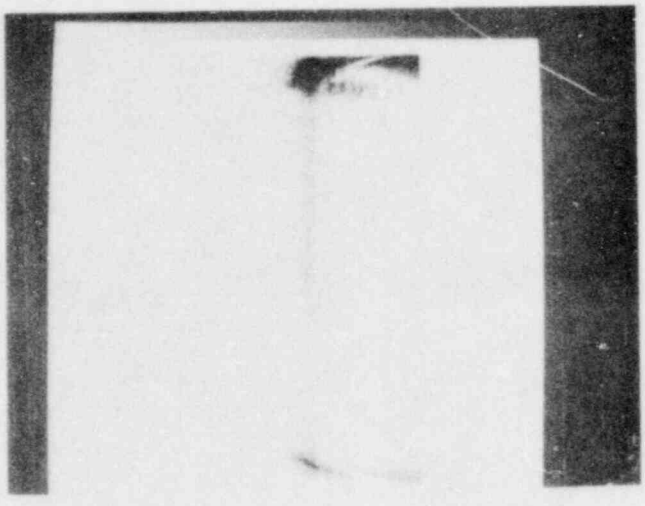

Figure 2.6a. Digital Computer Reconstruction of a Single SPR-II Illuminated LMFBR Fuel Pin.

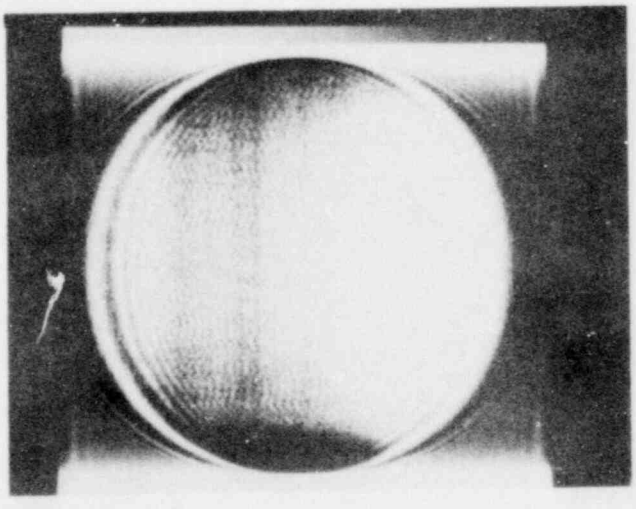

Figure 2.6b. Digital Computer Reconstruction of a 93% Enriched and a 20% Enriched LMFBR Fuel Pin Illuminated by the SPR-II.

Fourier transformed and the amplitude of the result is then output. The processing for these images is done row by row because the information is only encoded in one dimension (along a scan row).

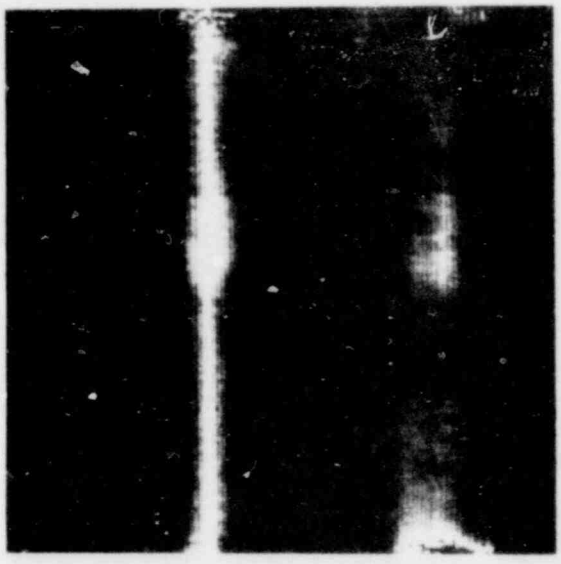

Figure 2.7. Reconstructed Image after Renormalization to Correct for Axial Power Variation in the Experimental Situation. (The reconstruction with the Fuel Pin in is on the Left. The Background-Only Picture is on the Right.)

Figures 2.6a and 2.6b show the SPR II images obtained for the single pin and double pin experiment respectively. The pseudohologram of the single pin experiment was scanned using a 256 x 512 array. The 512 pixels in the vertical direction represent a 150 mm high field of view at the fuel pin. The reconstruction in Figure 2.6a shows only the center 256 x 256 elements representing about a 75 mm section of the fuel pin. The second reconstruction, Figure 2.6b, was scanned using a 512 x 512 array. The two fuel pins used in this experiment can be seen in the center of the reconstruction. The strong signals

to either side of the fuel pin images in both Figures 2.6a and 2.6b are due to leakage in the collimator structure used in the experiment.

Figure 2.7 is a reconstruction of the coded images obtained in the ACPR experiments. The coded image shadowgrams were recorded on Kodak Type M x-ray Film and were scanned in a 256 x 256 mm format with each pixel being 0.385 mm high by 0.282 mm wide. The resultant reconstruction represents a field of view of about 185 mm in the vertical direction. The "pin-in" image is shown on the left in Figure 2.7. Inspection of the "pin-in" image shows the bright fuel pin image oriented vertically on a wider, less intense background area representing the scattered radiation from the PBE container. The intense vertical region in the center is caused by scattering from a steel flange which was present on the particular PBE container used in this experiment. The reconstruction on the right is of the PBE container without the fuel pin in place. This image shows the flange region and some of the PBE container, but the signal associated with the fuel pin is not present.

Figure 2.8 shows a radial scan from the region just above the flange. The solid line represents this "pin-in" situation, while the dashed line represents the "pin-out" experiments. Although it is tempting to simply subtract the "pin-out" image from the "pin-in" image, this has not been done to date because there is some uncertainty as to the relative magnitude between the "pin-in" and "pin-out" reconstructions. This is primarily due to uncertainty in the input exposure-net density characteristic used to change density to exposure values and was caused by unexpected differences in development temperature in the x-ray film processor used to develop the shadowgrams. Steps have been taken to correct this and true background subtraction should be possible in future experiments. An actual radial resolution of about 1.5 mm is indicated by these scans.

Figure 2.9 shows the initial reconstructions obtained by following the algorithm outlined previously. Because there was variation in the neutron and gamma fluence in the axial direction in the reactor as well as collimator cut-off toward the top and bottom of the image, the fuel pin image in Figure 2.9 appears to narrow at the top and bottom of the picture. To reduce this effect in an effort to produce better images and more accurate mass density mapping, the power profile along the pin is divided out of the data values producing the normalized images in Figure 2.7. The result of this procedure is that the images appear to be more uniformly structured over the whole vertical field of view. Figure 2.10 shows an axial scan which has been averaged radially over

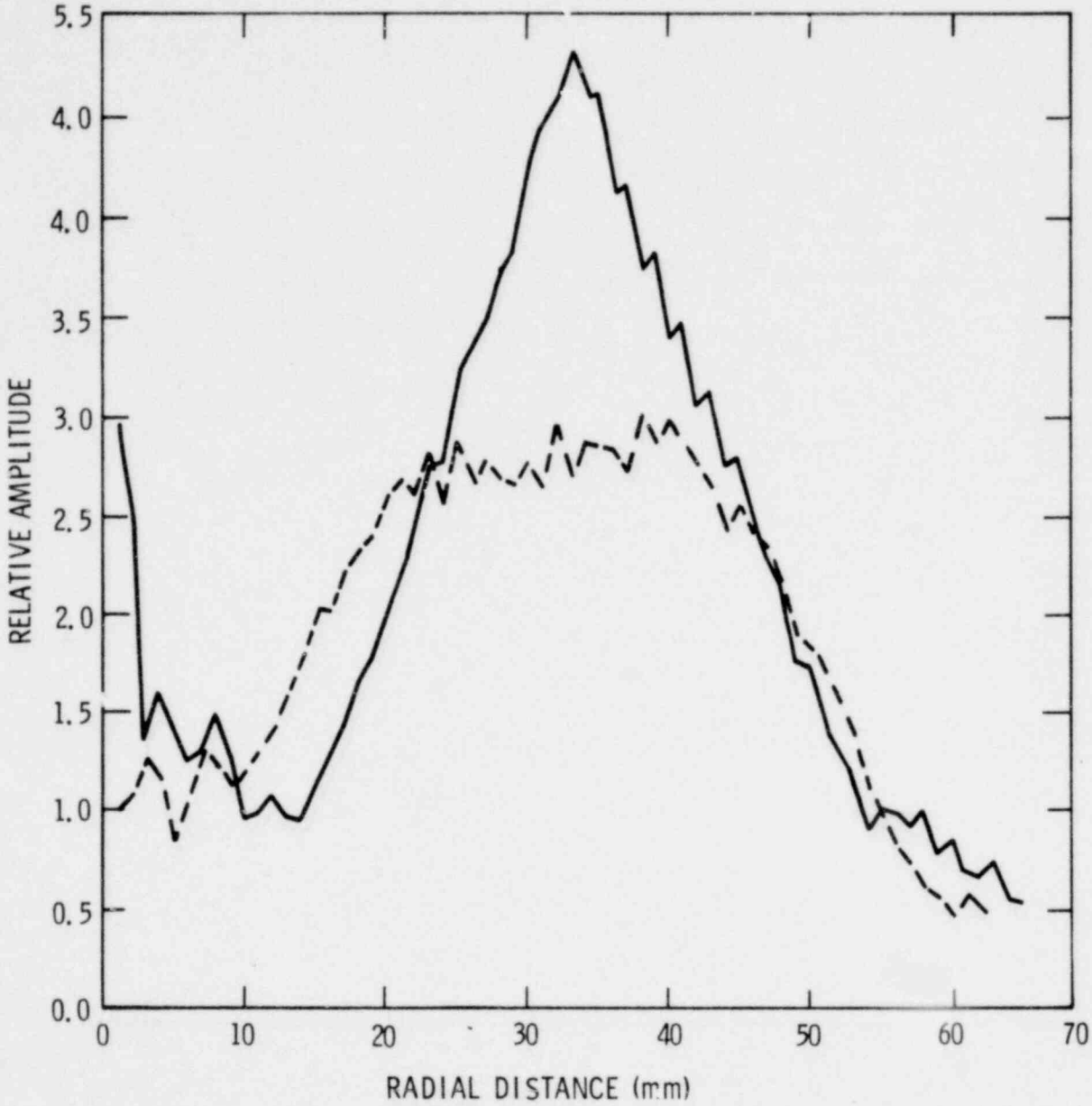

Figure 2.8. Power Profile in the Transverse Direction for the Pin In (Solid Line) and Pin Out (Dashed Line) Images.

the total fuel pin width. The dashed line is before normalization; the solid line is after normalization. Since the flange region was difficult to treat and will not be present in the final experimental configuration, no attempt at normalization was made in the flange region.

Figure 2.9. Reconstructed Images from ACPR Experiment (The Image on the Left Shows the Fuel Rod Centered on the Background Radiation from the Inconel Case and other Sources. The Image on the Right is the Inconel Case Alone.)

Some comparisons can be made between the digital and analog reconstruction techniques. The biggest advantage of the optical analog reconstruction is its speed. The reconstructed image is available immediately after the pseudohologram is placed in the optical system and many different combinations of d.c. blocking filters may be tried in rapid succession to optimize the image. The major disadvantage is that precise quantitative data from the optical image requires careful calibration of all steps of the photographic process. The digital reconstruction techniques offer a more linear reconstruction because the total process from original pseudohologram to output is linear and does

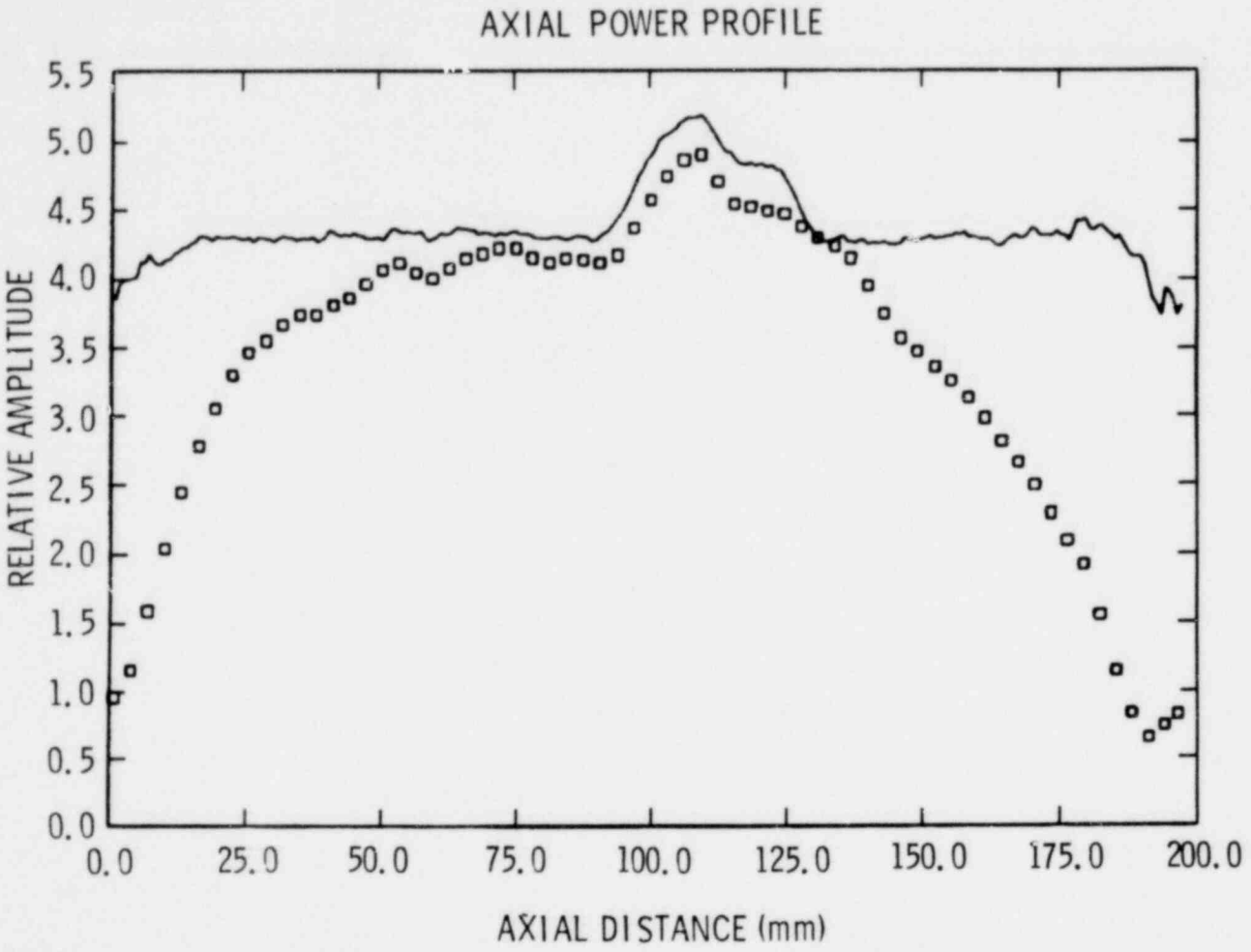

Figure 2.10. Axial Power Profiles Before Renormalization (Dotted Line) and After Renormalization (Solid Line) for Axial Power Variation Caused by the Reactor Flux Variation and Collimator Cut-Off.

1437 141

not require the nonlinear contrast enhancement step usually present in the analog reconstruction. Also, sophisticated background suppression techniques such as iterative background subtraction[3] can be easily accomplished in the computer. A further advantage is that codes other than the Fresnel zone plate (such as the uniformly redundant array[4]) may be reconstructed by using matched filtering or inverse filtering techniques. The disadvantage is that the digital reconstruction may take more time because of the digitization and computing time required.

The initial feasibility experiments at SPR-II and ACPR have shown that time resolved coded aperture images can be obtained in a reactor environment. By using both analog and digital means the image information has been extracted from pseudoholograms recorded at high background-to-signal ratios. Valuable experience has been gained in these experiments. Further improvement in both aperture design and reconstruction techniques should enhance the performance of the coded aperture imaging system even more.

REFERENCES

1. J. G. Kelly and K. T. Stalker, Proc. Int. Conf. on Fast Reactor and Related Physics, Chicago (1976). (In Print.)

2. K. T. Stalker and J. G. Kelly, Proc. SPIE/SPSE Tech. Symp. on X-Ray Imaging, 106-11, April (1977).

3. R. G. Simpson, H. H. Barrett, J. G. Kelly and K. T. Stalker, SPIE/SPSE Tech. Sump. on X-Ray Imaging, 106-12, April (1977).

4. E. E. Fenimore and T. M. Cannon, Applied Optics, to be published (1977).

CHAPTER 3

THE POTENTIAL FOR USING CODED APERTURE IMAGING FOR FUEL MOTION DETECTION MEASUREMENT IN THE STF

D. A. McArthur, J. A. Halbleib Sr., J. E. Morel, J. G. Kelly
Sandia Laboratories, Albuquerque, New Mexico

At Sandia Laboratories, coded aperture imaging of both neutrons and γ-rays is being investigated for fuel motion detection in STF as part of the NRC Reactor Safety Research program. Based on work done for the development of a fuel motion detection system for the ACPR UPGRADE, coded aperture imaging of γ-rays will be capable of producing high-resolution images of at least up to seven fuel pins. However, because of the short mean free path of γ-rays in the test fuel, it is not clear that γ-ray imaging can provide useful information in the large-bundle tests to be made in STF. Investigation of these questions in detail has therefore commenced using γ-ray transport codes. Alternatively, fast neutrons have a somewhat longer mean free path than γ-rays, and it may be desirable to image with fast neutrons in the case of larger fuel bundles. Discrimination against the large background signals from γ-rays and from low-energy neutrons (which have undergone considerable scattering) is necessary in fast neutron imaging. Conceivably, the additional sensitivity afforded by the coded aperture technique may allow use of a relatively inefficient threshold neutron detector (such as fast neutron induced fission in ^{238}U) to discriminate against these backgrounds, yet obtain useful images.

γ-ray transport calculations have been performed for a slab test fuel geometry which approximates a larger test fuel bundle ($\simeq$37 pins). These calculations yield both the uncollided fission γ-ray flux from the fuel, and the scattered gamma flux from the test fuel region and containment. These γ-ray fluxes have been used to calculate the expected signals in a realistic coded aperture imaging apparatus. By varying the construction of the coded aperture apparatus the effects of γ-ray filters on the signals from various portions of the test region can also be determined.

The γ-ray calculations employed realistic material compositions and detailed γ-ray cross-sections available in state-of-the-art transport codes. Only the scattering and absorption of fission γ-rays emitted by the test fuel were treated. Scattered γ-rays from the driver

reactor core and γ-rays resulting from neutron capture in the test section were neglected. For the initial fission γ-ray spectrum emitted by the test fuel, a measured spectrum for ^{235}U fission was used.[1]

A modified version of the Sandia Laboratories Monte Carlo transport code TIGER[2] simulated transport within the test section, approximated by the slab geometry of Figure 3.1. TIGER, which calculates the radiation emitted from the slab geometry, was modified to tally separately the point of origin of unscattered radiation, or the position of last scatter for scattered radiation. This detailed spectral information permits the calculation of coded aperture signal components originating from deep within the fuel bundle, or from scattering in the containment.

5

Figure 3.2 shows the mockup of the coded aperture system which includes an optional γ-ray filter, three zones of a circular zone plate of arbitrary thickness and composition, and a detailed mockup of a typical commercially-available sodium iodide scintillator. Collimators present in typical coded aperture systems restrict the angular range of incident photons to that shown in Figure 3.2.

The coded aperture signals are proportional to the spatially-modulated component of the energy deposition in the sodium iodide scintillator. The point γ-ray source represents the unscattered, scattered, or total emission from any region of interest in the test section slab geometry, where the radiation intensity and spectrum are obtained from the TIGER calculations. Transport through the coded aperture system to the scintillator is calculated with the Sandia Laboratories code CYLTRAN.[3] Several options in CYLTRAN were used to reduce variance and minimize running time.

Figure 3.3 shows typical results from TIGER for an undisturbed fuel region geometry. The photon emission decreases by about a factor of ten in going from the row of fuel pins nearest the coded aperture system to the row farthest from the system. Scattered radiation is an important component of the emission from the test fuel, but is never more than 30 percent of the total emission, and decreases in importance for the deeper regions in the test fuel.

There is also a very large emission component resulting from scattering in the steel containment walls. This radiation is considerably softer than the desirable radiation from the test fuel (average energy ≈0.8 MeV versus ≈1.5 - 2 MeV). Therefore a high-Z γ-ray filter in the coded aperture system should help discriminate against this scattered component. Figure 3.4 shows the coded aperture signal calculated

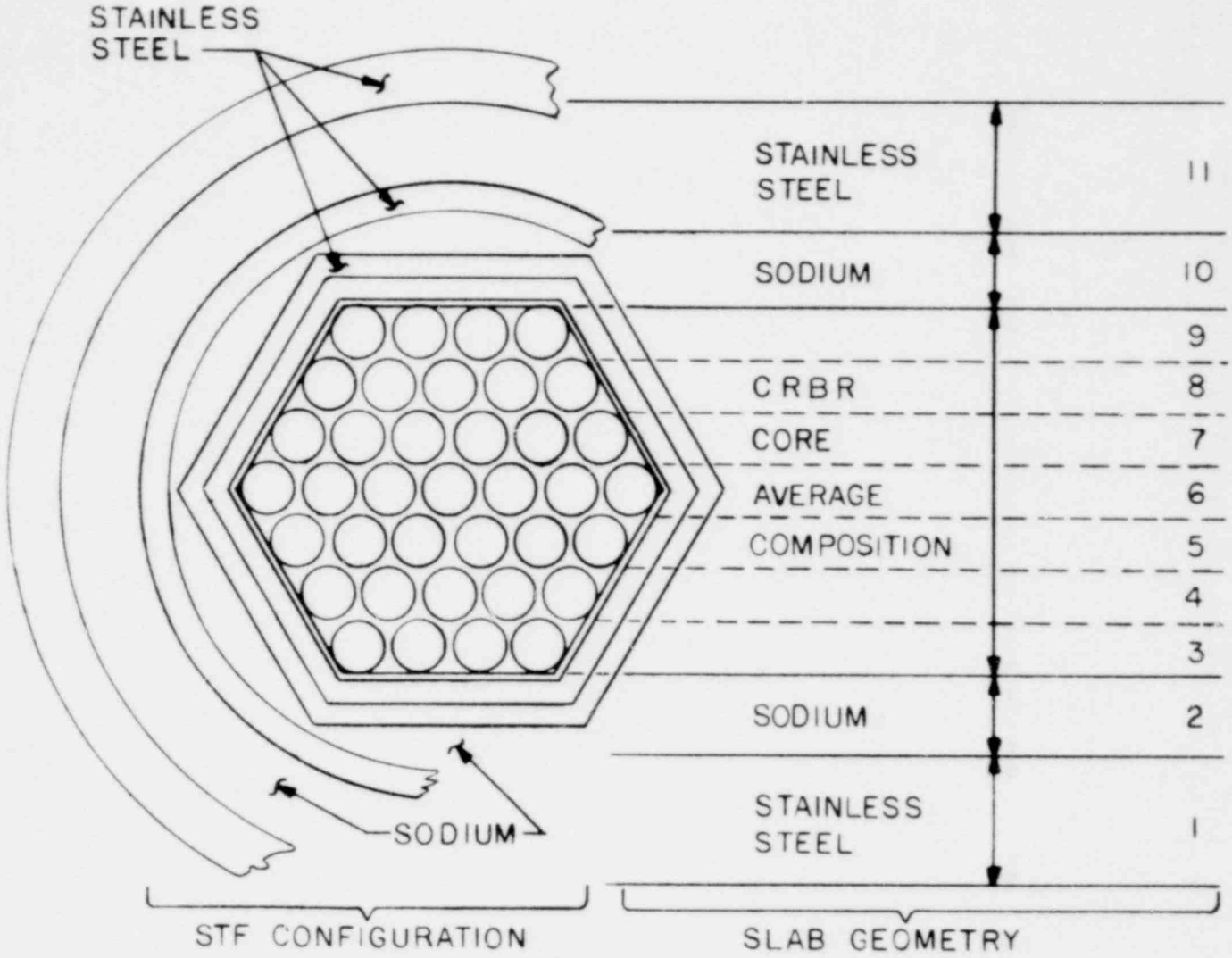

Figure 3.1. 37-Pin Bundle in the STF Small Package Loop, Together with the TIGER Slab Approximation.

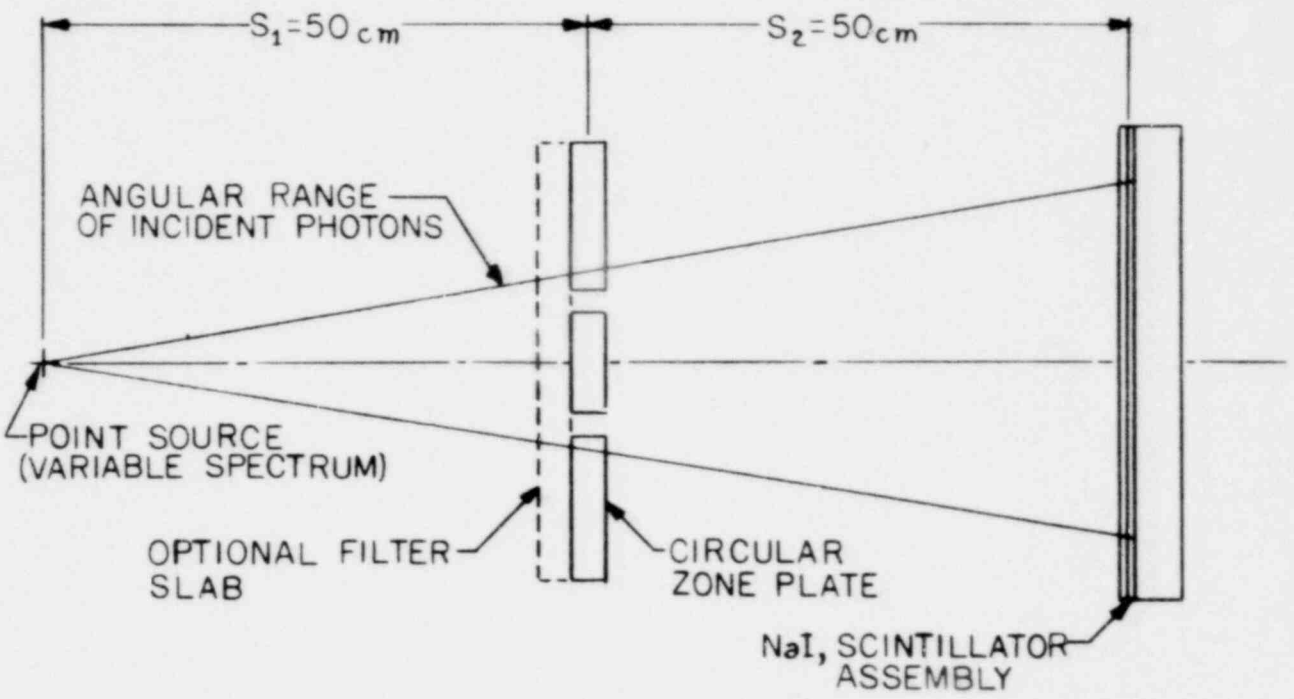

Figure 3.2. Coded Aperture System Geometry Used in CYLTRAN.

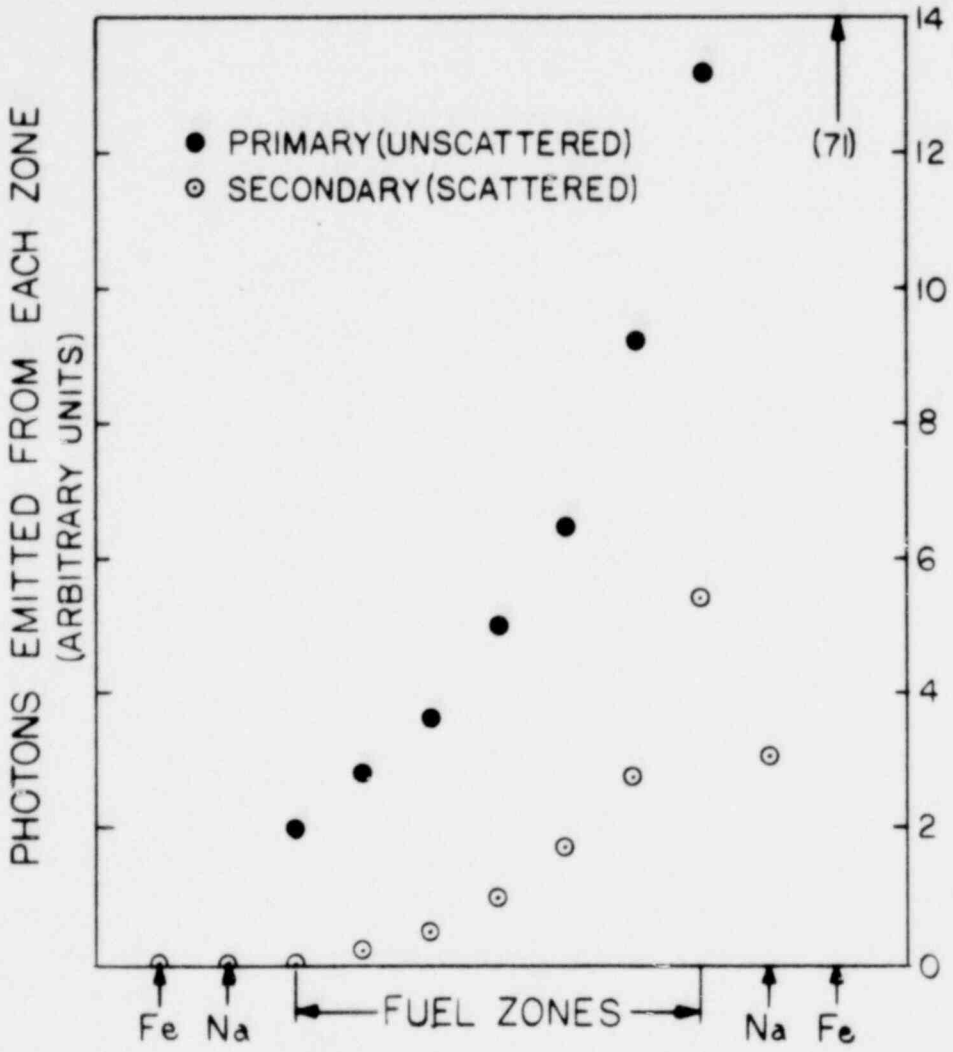

Figure 3.3. Unscattered and Scattered Photon Emission from the 37-Pin Bundle and Containment as Calculated with TIGER. Each Zone Represents a Row of Fuel Pins in the 37-Pin Bundle.

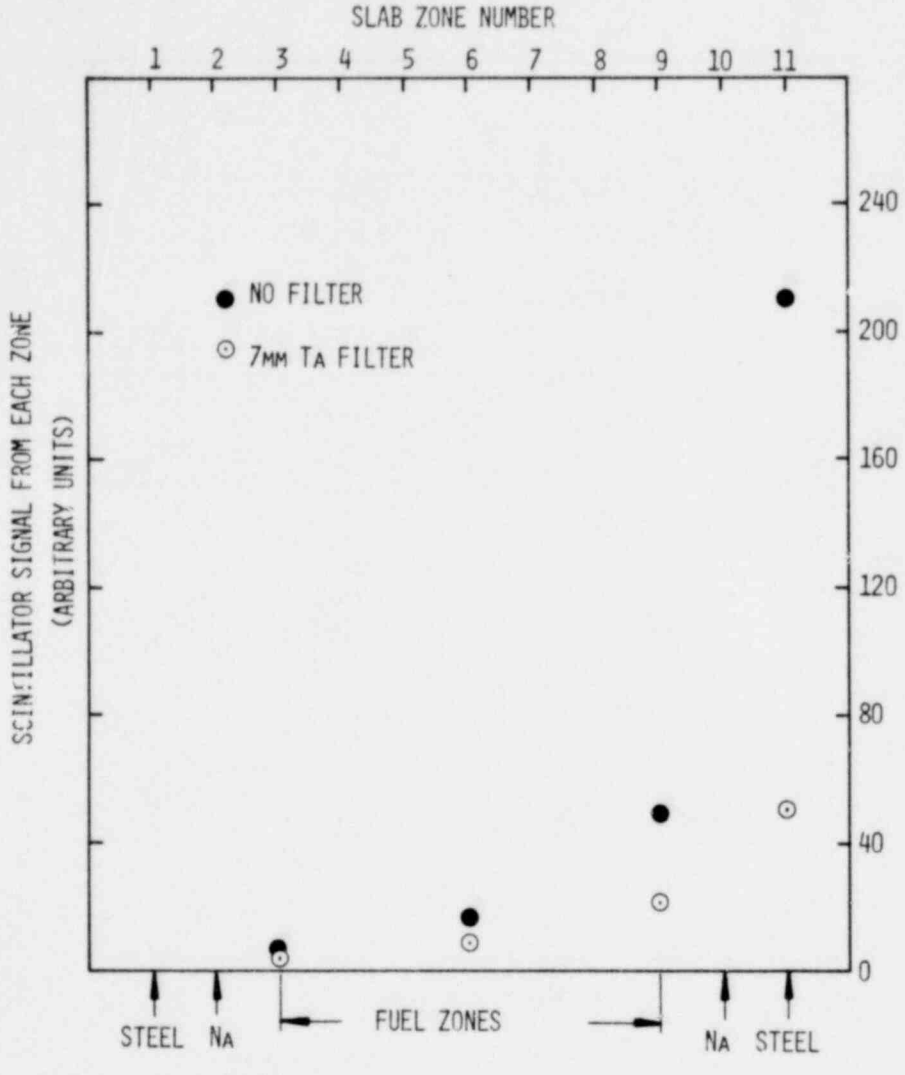

Figure 3.4. Coded Aperture Signal in the NaI Scintillator for Emission from Various Regions of the Test Section.

with CYLTRAN (for a Ta zone plate 1.27 cm thick), for either no filter or a 7 mm Ta filter in the coded aperture system. The Ta filter attenuates the scattered component from the steel about twice as much as it does the desired signal from the fuel regions, thus increasing the relative magnitude of the desired signal.

The changes in photon emission and in the coded aperture signal resulting from partial voiding of fuel from the test section have also been calculated. To approximate voiding of a single fuel pin, all the material was removed from one of the zones of the fuel region. TIGER calculations show that γ-ray emission from the voided region is partially compensated by greater emission from those zones behind the voided region, because there is now no attenuation in the voided region (Figure 3.5). The scattered component from the steel containment also decreases somewhat. Introducing a 7 mm Ta filter into the coded aperture system also enhances the coded aperture signal change caused by fuel voiding.

In summary, the calculated coded aperture signal magnitudes are approximately as large as those observed by Kelly[4] in a similar geometry in the ACPR. Scattered radiation from the containment thickness assumed here is large, but its magnitude can be reduced with a high-Z γ-ray filter. The scattered radiation from the test fuel is a relatively small component of the total emission except for those rows of fuel pins nearest the coded aperture system. A high-Z filter in the coded aperture system also enhances the signal change resulting from fuel voiding.

Future work in this area will include use of these codes to optimize the coded aperture design, to study voiding of larger amounts of test fuel, and to study loss of sodium and steel from the test fuel region. A more accurate treatment of the scattering is also planned, through the use of non-slab geometries in the test section. Finally, the neglected components of capture-γ radiation and scattered driver-reactor-core radiation will be studied, although these components are not expected to be dominant based on preliminary experimental results of Kelly. Experimental verification of the calculational results is also planned.

The neutron imaging work performed thus far is primarily experimental and is intended to investigate the feasibility of developing a coded aperture system which is sensitive primarily to neutrons with energies $\geq$ 1 MeV. The most important potential problems appear to be (1) development of coded apertures with high spatial resolution which are able to modulate the fast neutrons sufficiently and (2) development

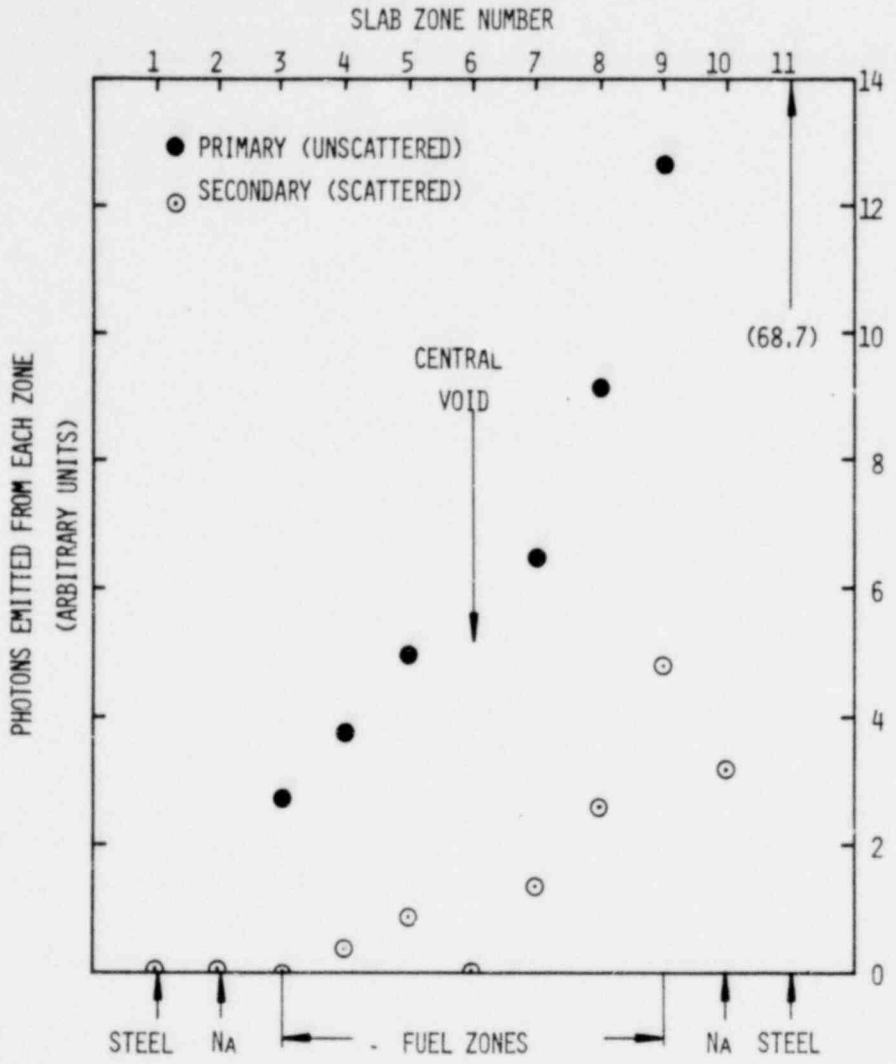

Figure 3.5. Effect of Fuel Voiding from the Central Fuel Zone on the Photon Emission from the Test Section.

of a transient two-dimensional detector system which is insensitive to γ-rays and has a detection efficiency high enough to produce useful images. If the coded aperture must be very thick to modulate the neutrons, it will have a narrow field of view, which is undesirable. Low-angle scattering of neutrons from the sides of the coded aperture elements is also of concern. Therefore it is important to measure which coded aperture materials are optimum and how fine the structure in the coded aperture can be made. For the transient detector, several systems can be envisioned, but their feasibility depends on unknown parameters such as the efficiency of light emission from scintillators irradiated by fission fragments. Work is therefore being performed in both areas.

The initial fast neutron detection method chosen was fast-neutron-induced fission in ^{238}U, which is sensitive to neutrons with energies $\geq$ 1.5 MeV. To eliminate γ-ray and alpha particle backgrounds during fast neutron modulation experiments, the fission fragments have been detected initially by the damage tracks they produce in Lexan plastic.

Figure 3.6 shows a typical fast neutron modulation experiment with the Sandia Laboratories ^{252}Cf spontaneous fission source. Slabs of a candidate neutron coded aperture material (such as steel, polyethylene or tungsten) are placed between the source and the sheet of depleted uranium in contact with the Lexan. Only fission fragments produce a high enough ionization density in the Lexan to produce etch pits. The Lexan is exposed in contact with the depleted uranium, and is then etched in a caustic solution. The resulting etch pits are visible because they scatter light, and the scattered light intensity is proportional to the fast neutron fluence at that point on the detector.

Using the apparatus of Figure 3.6, clear fast-neutron shadows have been observed for 2.5 cm thick slabs of materials such as polyethylene, steel, and tungsten alloy. The widths of the slabs have been as small as 3 mm, without any apparent loss of definition in the shadow cast by the material. The degree of neutron modulation appears to agree reasonably well with simple theory. The scattered light patterns are sufficiently intense that they may be photographed. The photography should lead to photoreduced images suitable for holographic reconstruction.

Future work in this area will emphasize the reconstruction of ^{252}Cf source images using coded apertures similar to those required for fast reactor safety experiments, and development of transient detector concepts. Much can be learned about the properties of neutron images

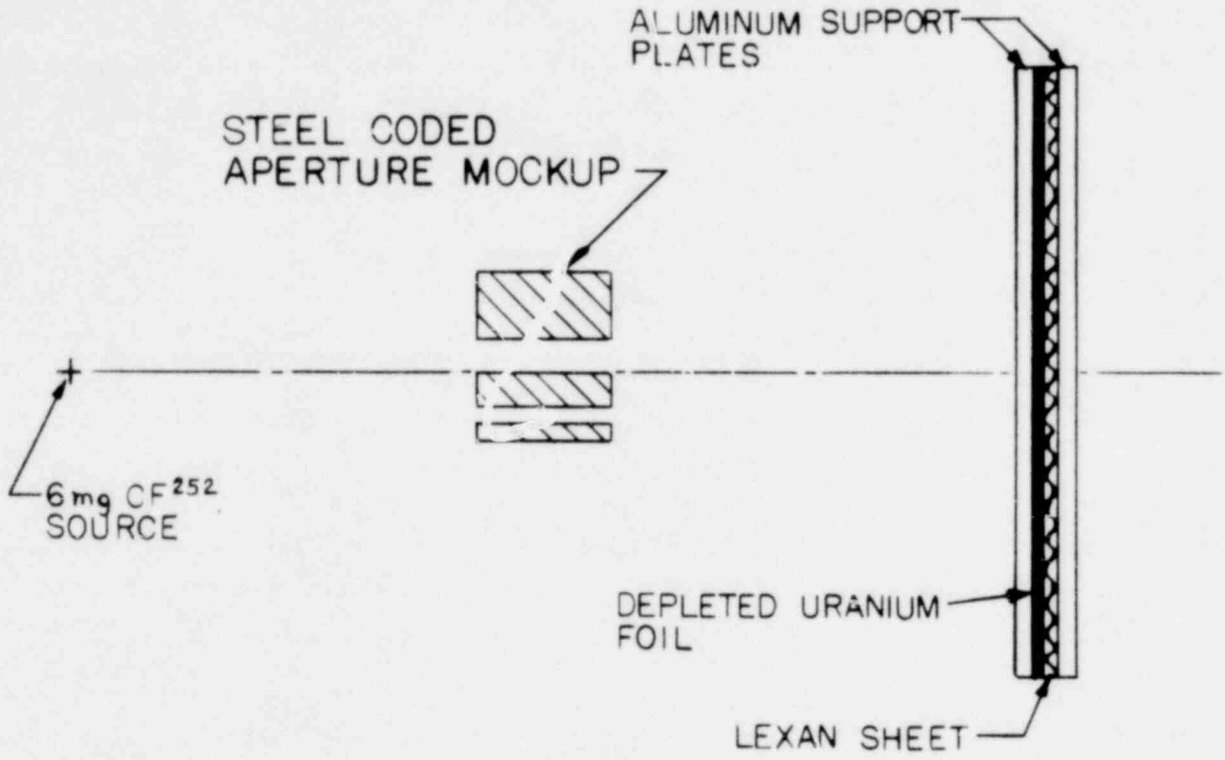

Figure 3.6. Typical Experimental Geometry for Fast Neutron Modulation Experiments with the Sandia ^{252}Cf Source.

with the static Lexan track detector, so this technology will also be improved. Further, theoretical studies will be carried out on various alternate threshold fast neutron detectors.

REFERENCES

1. V. V. Verbinski, H. Weber and R. E. Sund, Phys. Rev. C, 7, 1173 (1973).
2. J. A. Halbleib, Sr. and W. H. Vandevender, Nucl. Sci. Eng. 57, 94 (1975).
3. J. A. Halbleib, Sr. and W. H. Vandevender, Nucl. Sci. Eng. 61, 288 (1976).
4. J. G. Kelly and K. T. Stalker, Trans. Am. Nucl. Soc. 27, 512 (1977).

CHAPTER 4

THE RELATION BETWEEN FUEL MOTION AND DETECTOR RESPONSE FOR IN-CORE FUEL MOTION DETECTION SYSTEMS

P. J. McDaniel, S. A. Wright
Sandia Laboratories, Albuquerque, New Mexico

W. H. Scott, Jr.
Science Applications, Inc., La Jolla, California

The detection of fuel motion within test sections of reactors which have no slots (SLSF, EBR-II, SCARABEE) requires the use of an in-core fuel motion detection system. In-core systems can also be useful as auxiliary fuel motion monitoring systems for reactor facilities which do have slots. A supplementary in-core fuel motion detection system would be especially useful for large-bundle tests, since self-shielding effects may degrade the resolution of external viewing systems.

With support from the U. S. Nuclear Regulatory Commission, an experimental program is being conducted at Sandia to demonstrate the feasibility of in-core fuel motion detection systems. This program has two major developmental efforts. The first requires development of a suitable set of detectors, and the second requires development of analytical methods which can determine fuel motion from detector signals.

An experimental verification of the detector operation and the analysis system will be provided by a series of static tests on 7-, 19-, and 37-pin fuel bundles placed in the center of the Sandia Pulsed Reactor (SPR-III).[1] Following these experiments, 1- and 7-pin dynamic tests will be performed in Sandia's Annular Core Pulse Reactor (ACPR) during the Prompt Burst Excursion (PBE) experiments.[2] Figure 4.1 shows the 37-pin test assembly to be placed in SPR-III. For various fuel configurations, the fuel bundles will be pulsed by the reactor and the detector responses measured. Actual fuel displacements from the unperturbed configuration will be unfolded from the detector data. The unfolded fuel configuration can be compared with the known configuration to determine the accuracy of the technique.

The detector development to date focuses on an intrinsically heated fission-thermocouple type detector, 4 mm long and 1.5 mm in diameter. The fissioning material is ^{238}U in a U10Mo alloy.[3] Thus the detectors are primarily sensitive to fast neutrons. The small size of the detectors allows approximately 40-50 detectors to be placed in, and around, the 37-pin test assembly. Additional types and sizes of detectors are

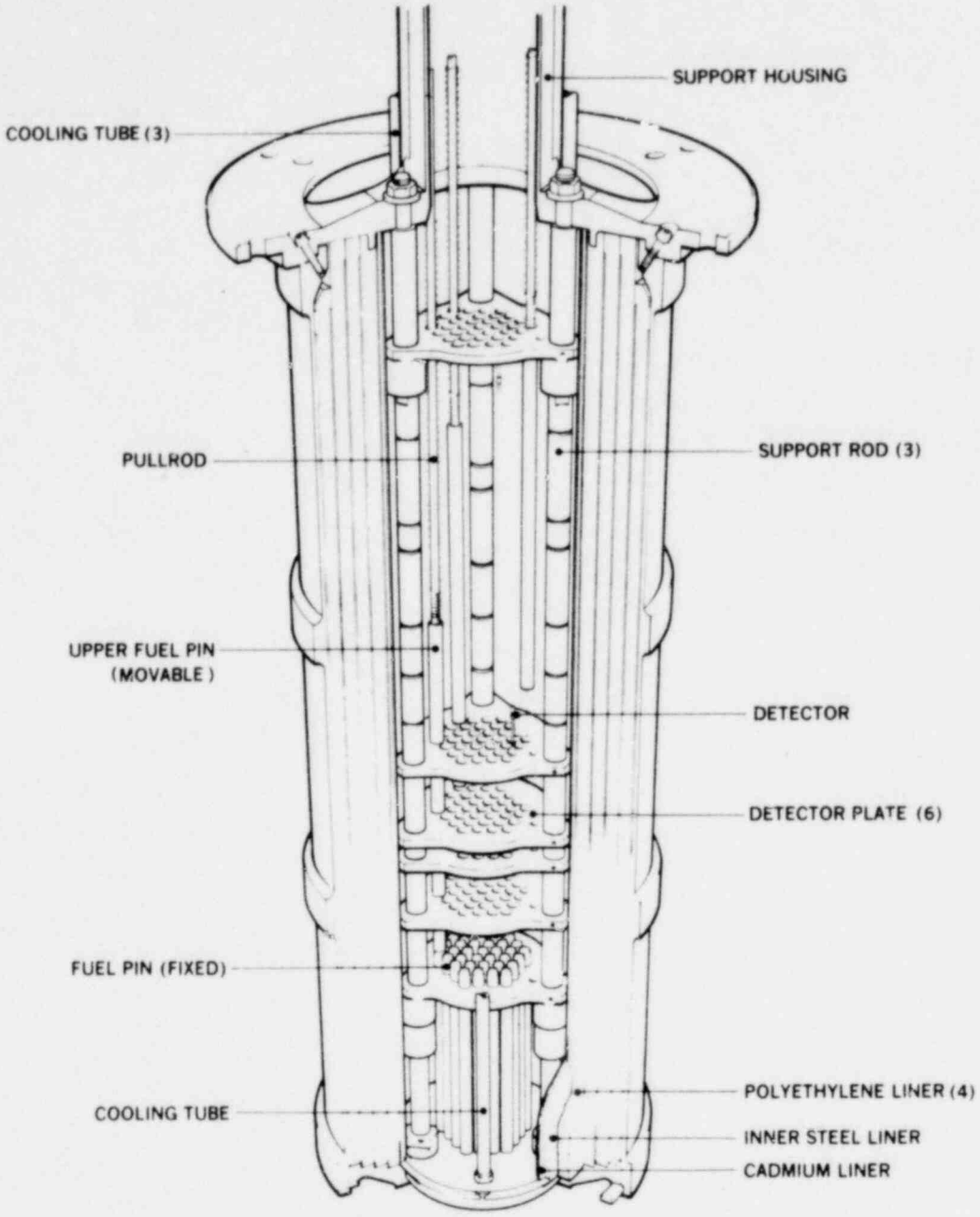

Figure 4.1. 37-Pin Test Assembly for the SPR-III Experiments.

also being considered. They include diamond semiconductor detectors,[4] platinum self-powered detectors,[5] and miniature fission chambers operating as self-powered detectors.[6]

The development of analytical techniques requires relating detector responses to fuel motion. The change in the response of the detector due to fuel movement is a result of two competing effects. When fuel is moved away from a detector, fewer neutrons reach the detector due to a loss of source neutrons provided by the fuel. However, in opposition to this effect, more neutrons reach the detector due to a loss of shielding provided by the fuel. For a ^{238}U detector located in a fast reactor, the first effect dominates. These two effects can be treated by applying perturbation theory to the neutron transport equation and its adjoint. The change in response of detector $i(\Delta R_i)$ due to a fuel movement within fuel volume $j(V_j)$ is given by the equation[7, 8, 9]

$$\Delta R_{ij} = \int_{V_j} \int_{\tau} \phi_i^* \int_{\tau'} \delta\Sigma_s(\tau' \rightarrow \tau)\, \phi \, d\tau' \, d\tau \, dV \qquad (1)$$

$$- \int_{V_j} \int_{\tau} \phi_i^* \, \delta \, \Sigma_T \, \phi \, d\tau \, dV$$

where

ϕ = The angular flux density solution to the transport equation.

ϕ_i^* = The adjoint angular flux density for an adjoint source at detector i.

$d\tau$ = An elemental volume in energy-angle phase space.

$\delta\Sigma_s$ = The change in the neutron production in phase space $d\tau$ due to fuel movement in volume V_j (includes fission and scattering sources).

$\delta\Sigma_T$ = The change in neutron destruction in phase space $d\tau$ due to fuel movement in volume V_j.

This equation can be put into a form better suited for fuel motion detection by assuming that the changes in the macroscopic cross sections are caused only by fuel density changes ($\delta\Sigma = \Delta\rho\sigma$). Thus

$$\Delta R_{ij} = K_{ij} \Delta \rho_j \tag{2}$$

where

$$K_{ij} = \int_{V_j} \int_{\tau} \phi_i^* \int_{\tau'} \sigma_s (\tau' \rightarrow \tau) \phi \, d\tau' \, d\tau \, dV$$

$$- \int_{V_j} \int_{\tau} \phi_i^* \sigma_\tau (\tau) \phi \, d\tau \, dV \tag{3}$$

$\Delta \rho_i$ = The density change in volume V_j.

The term K_{ij} is called the detector response kernel and is used to relate the i^{th} detector response to the fuel density changes in volume V_j. The total change in the detector response is obtained by summing ΔR_{ij} ver all volumes.

$$\Delta R_i = \sum_j \Delta R_{ij} = \sum K_{ij} \Delta \rho_j \tag{4}$$

This equation is known as the unfolding equation since ΔR_i is known through measurements, K_{ij} is known through calculations, and $\Delta \rho_j$ must be determined.

To determine the detector response kernels, the forward and adjoint fluxes must first be determined.

The complexity of the test-assembly geometry and the asymmetric location of the detectors required calculating the angular flux density and adjoint angular flux density in 3 dimensions. This is accomplished with the general Monte Carlo code MORSE. Figure 4.2 illustrates the magnitude of a detector response kernel for a point detector located in the coolant channel next to a fuel pin. Notice that it is very local and falls off approximately as $1/r^2$. This result is significant, since it implies that the resolution of in-core fuel motion detection systems can be quite good. However, it also implies that a large number of detectors must be used, and they must be close to the fuel if high resolution is to be achieved.

In addition to calculating the detector response changes using the adjoint flux technique, the unperturbed detector response can also

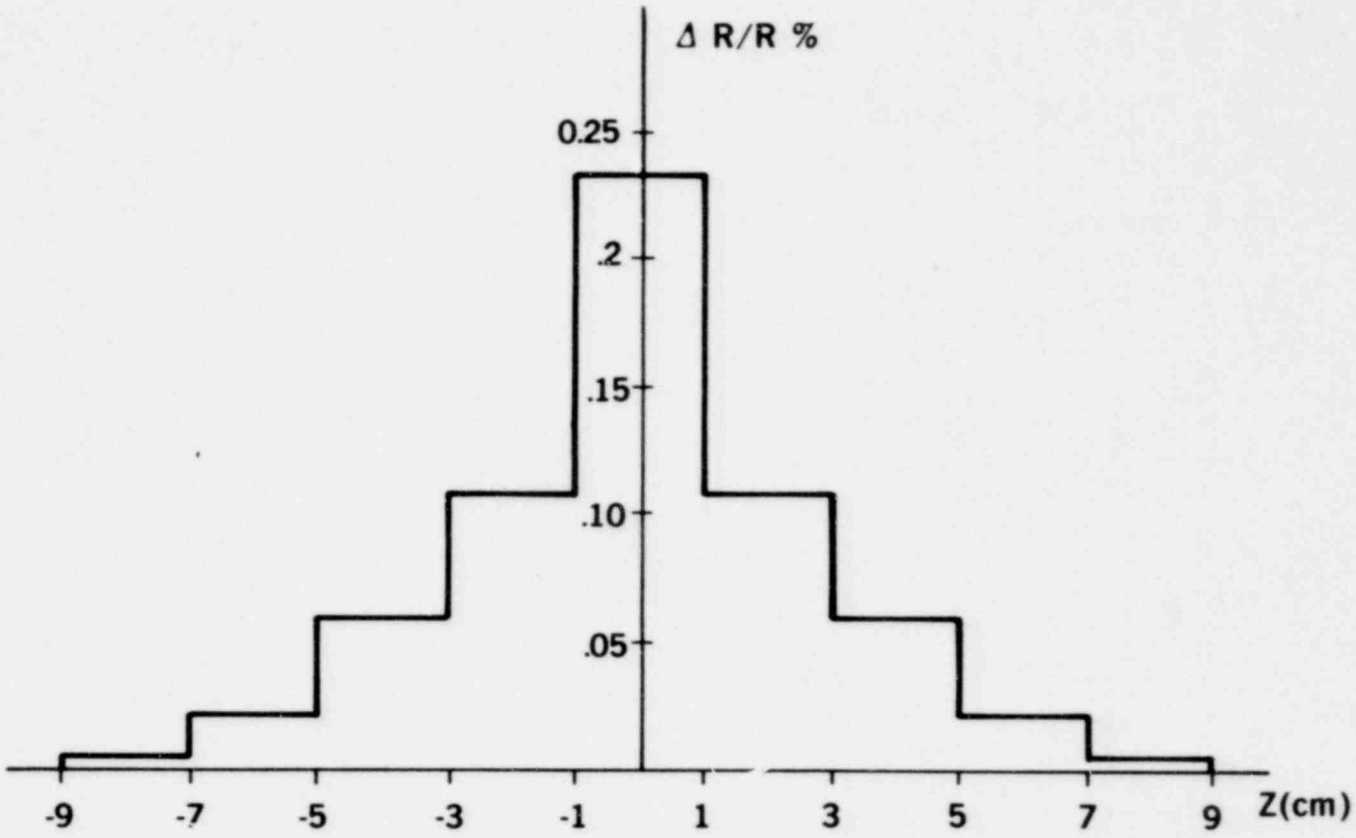

Figure 4.2. Percent Change in Detector Response as a Function of Axial Distance away from a Point Detector.

be calculated using adjoint fluxes. It is calculated as an integral of the forward angular flux times the adjoint angular flux over a coupling surface which encloses the test assembly. This technique is more accurate than the simple activation integral based only on the forward neutron flux density.

To demonstrate the validity of this technique for determining detector responses, direct (forward) calculations of the detector responses were made for unperturbed and perturbed fuel geometries. The same fuel geometries were then used to calculate detector responses using the adjoint flux (perturbation) procedure. The model chosen for this evaluation approximated the geometry of the 7-pin SPR-III experiments. In this model 12 detectors were located between the center pin and 6 outer pins. Twelve other detectors were located just outside the outer row of pins. The detectors were located 20 mm apart axially. Figure 4.3 shows a comparison of the detector outputs calculated by the direct method versus the perturbation method. In the perturbed geometry, the top 150 mm portion of all 7 pins is displaced upward 80 mm. The two curves represent the flux at the inner detector locations for the unperturbed and perturbed cases as calculated by the direct method. The circles represent the unperturbed detector responses calculated by coupling the forward and adjoint fluxes at a surface surrounding the test assembly. The triangles represent the perturbed detector responses as calculated from perturbation theory. The agreement between the perturbation procedure and the direct calculation is quite good.

Having confirmed the adequacy of the response-kernel generation technique, unfolding procedures were developed to invert the detector response matrix (defined in equation 4). This procedure is based on a singular value analysis of the response kernels and a limiting of the solution space for fuel movement to physically real possibilities.[10,11] Four types of information are available for the unfolding. The response kernels and detector responses provide one set of information. An additional set of information is available in terms of inequalities that the fuel movement must satisfy. Non-negative fuel density is an example of such an inequality. A third set of information is provided by known physical laws. Conservation of mass is an example. The fourth set of information takes the form of intuitive guesses as to the nature of the fuel movement. These intuitive constraints require the fuel motion to be not too different from some physical model of the motion.

In order to analyze the data that will be generated by the SPR-III and ACPR experiments, two computer codes were written to calculate the

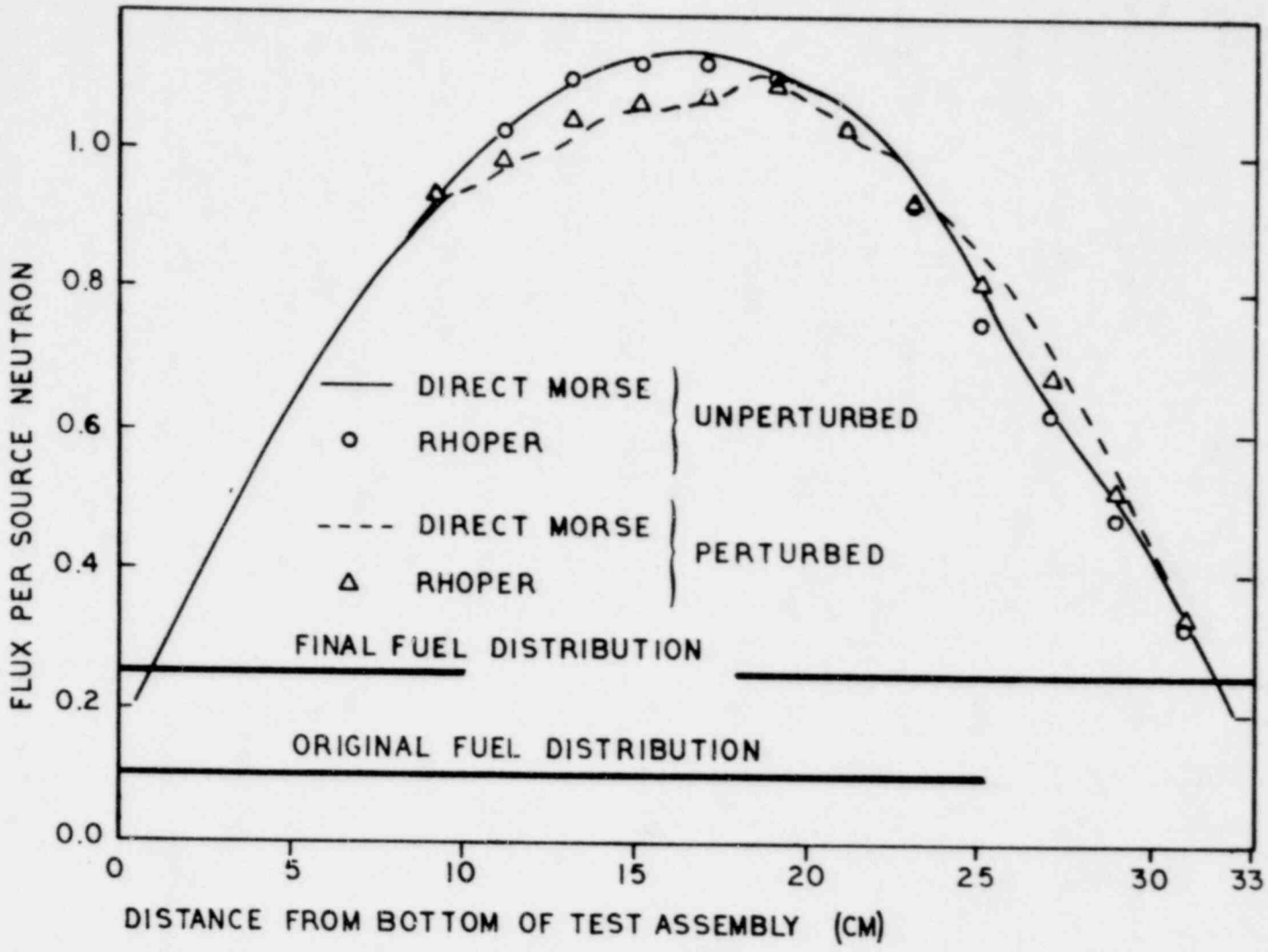

Figure 4.3. Perturbed and Unperturbed Detector Responses Determined from Forward Transport Calculations and Perturbation Theory.

necessary kernels and unfold the measured data. The code RHOPER generates the kernels from the results of forward and adjoint MORSE calculations; it was used in the preceding section to calculate detector responses. The code MOVUN takes the kernels generated by RHOPER and the experimental data, applies the given constraints, and unfolds the measured fuel movement. It also provides an error estimate for the unfolded fuel movement within each subvolume of the test assembly.

A number of sample problems were run to estimate the fuel movement resolution possible with the in-core detectors and the RHOPER/MOVUN analysis scheme. Simulated data was calculated by RHOPER and provided to MOVUN. MOVUN perturbs these data with random errors having a gaussian distribution with standard deviation equal to 2% of the unperturbed signal. These data are then treated as experimental values. An example of an unfolded result is provided in Figure 4.4 for the fuel movement described in Figure 4.3. All 7 pins were lumped together radially and then the upper part of the subassembly volume was divided into 12 axial bins. In the initial configuration, fuel occupied the lower 8 bins with a density of 1.0. The upper 4 bins were empty. The bottom part of the subassembly (lower 100 mm of fuel) contained no detectors, and therefore, it was not considered in the unfolding analysis. Figure 4.4a presents the final densities and Figure 4.4b presents the density changes. The unfolded fuel distribution agrees quite well with the actual distribution. The error estimates on the unfolded result correspond to approximately a constant 30% of the initial fuel density in each bin. For this problem each volume bin corresponds to approximately 45 g of fuel and the estimated error in each bin corresponds to about ± 13 g of fuel.

Similar sample problems were run to estimate the fuel mass resolution as a function of the signal-to-noise ratio (SNR). In these calculations the SNR was varied from two to four. The fuel densities and their standard deviations were calculated for each volume bin, however, 10 volume bins were used instead of 12. Figure 4.5 shows the standard deviation of the unfolded fuel mass in each volume bin. As expected increased SNR's improve the resolution capabilities of the unfolding techniques; in fact resolution appears to be inversely proportional to the SNR. To estimate the resolution capabilities of the SPR-III experiments, the SNR's of the fission couple detectors were measured. Assuming an average signal equal to 5% of background, the SNR for the SPR-III experiments should be in the range of 5-10. Such high values of SNR will provide excellent fuel mass resolution, probably on the order of 5-10 g.

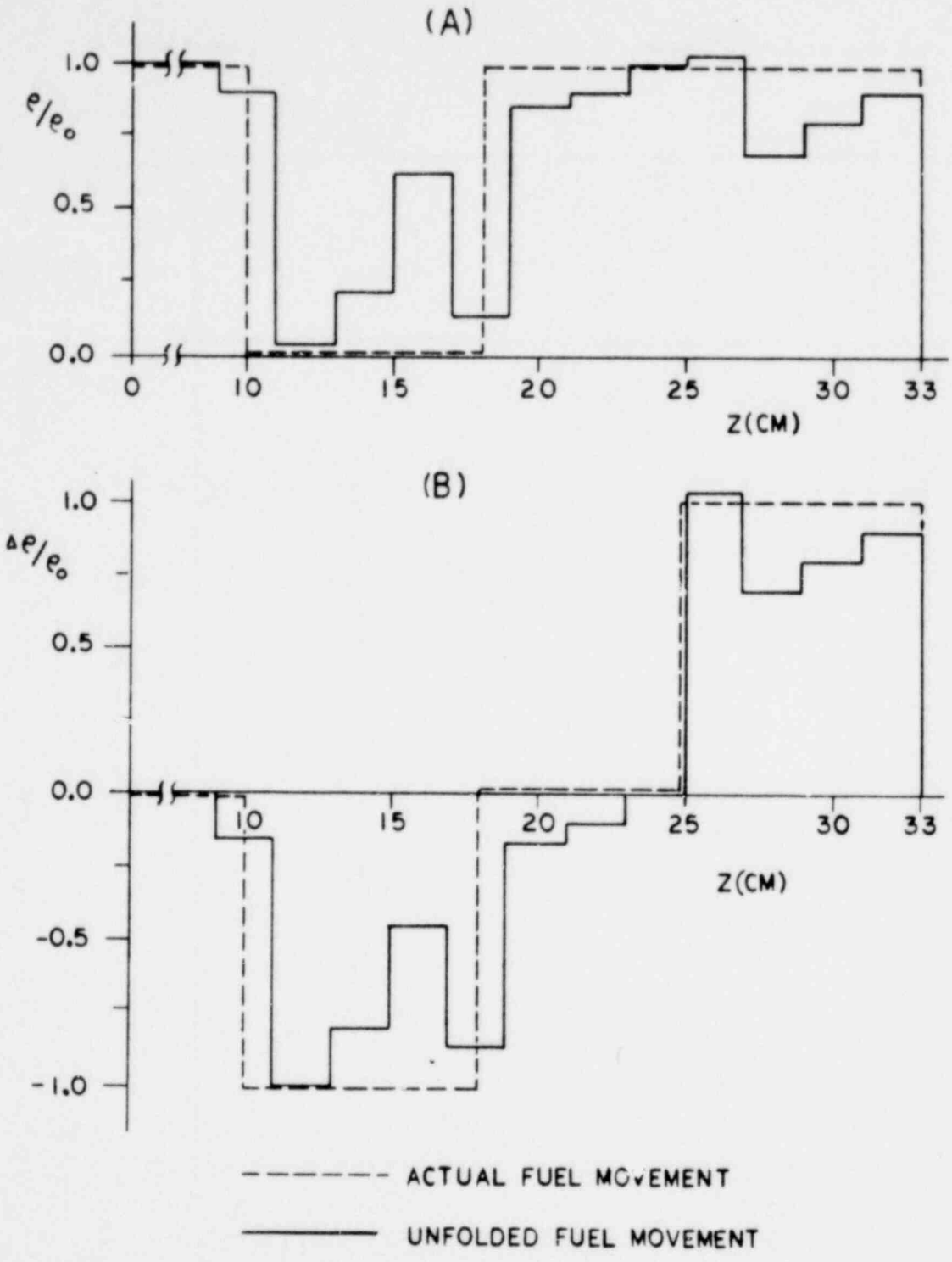

Figure 4.4. Unfolded Fuel Motion for Simulated Data Having a Signal-to-Noise Ratio of 2.5.

1437 164

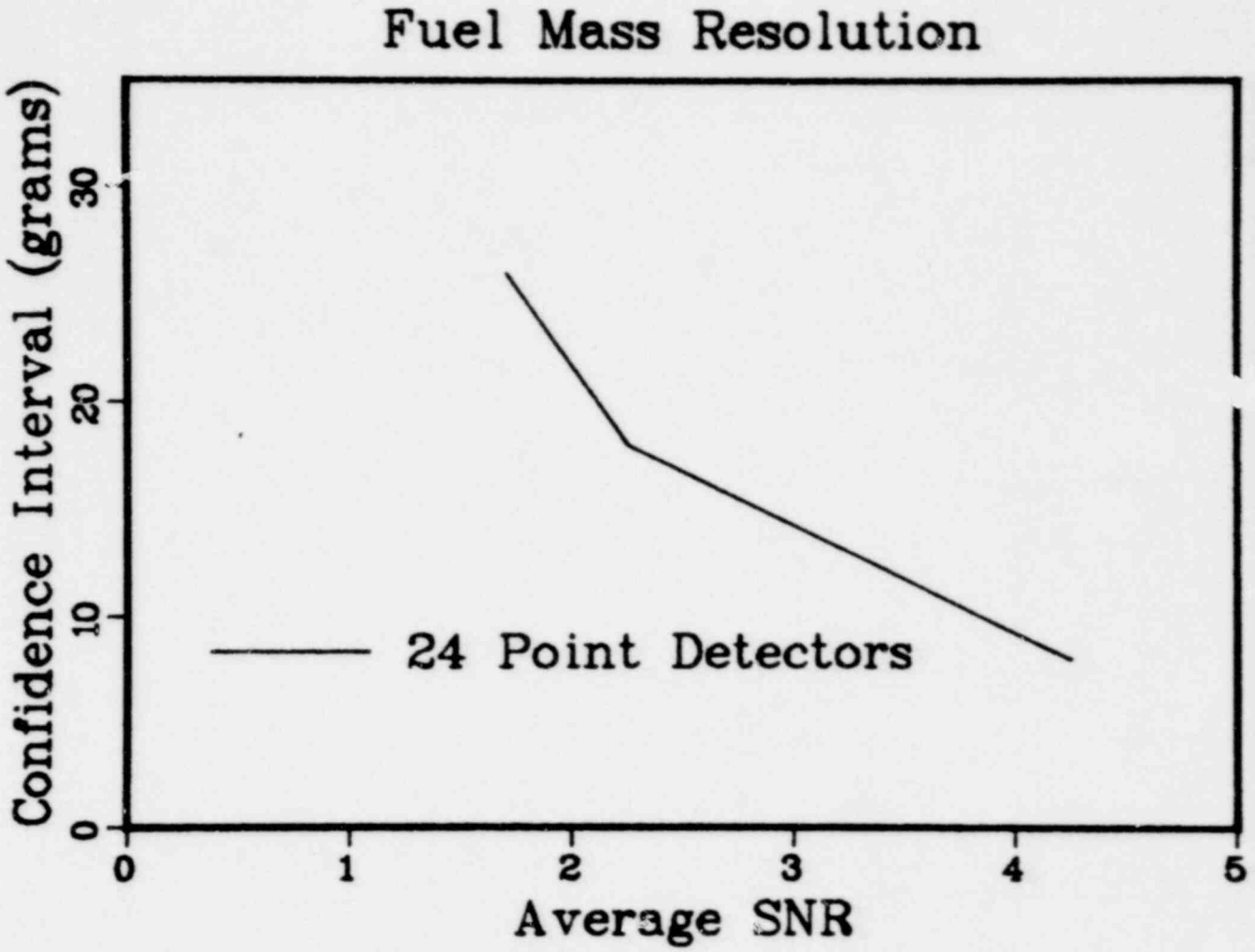

Figure 4.5. Fuel Mass Resolution in 53 Gram Subdivisions of a 7-Pin Bundle.

The sample problems described in this report represent a complete simulation of in-core fuel motion detection. It was shown how one can generate accurate detector response-kernels using perturbation theory and how simulated data for specific fuel perturbations could be unfolded to determine the fuel distribution. A comparison of the unfolded fuel distribution agreed very well with the actual fuel distribution and indicated that the resolution capabilities of the in-core fuel motion detection system for this small test assembly can be as small as 5-10 g.

In conclusion two points must be stressed. First, based on these calculations, it appears that the resolution capabilities of in-core fuel motion detection systems may be much better than anticipated. Second, the method of analysis used here to generate detector response-kernels and unfold data is in no way limited to in-core fuel motion systems. In fact with little or no modifications to our codes, similar sample problems could be performed for both coded-aperture systems and hodoscope systems. The final conclusions regarding the feasibility of in-core fuel motion detection systems however, must still await the SPR-III and ACPR experiments.

REFERENCES

1. Fast Reactor Safety Research Program-Quarterly Report, April-June, 1976, SAND-76-0273, Sandia Laboratories, Albuquerque, New Mexico (1976).

2. Experimental Fast Reactor Safety Research Program Quarterly Report January-March, 1975, SAND-75-0225, Simulation Sciences Research Dept., Sandia Laboratories, Albuquerque, New Mexico (1975).

3. R. G. Morrison and D. B. Stillman, Fission-Couples Applied Toward Reactor Diagnostics and Safety, Los Alamos Scientific Laboratories, LA-3470-MS, TID-4500 (1966).

4. R. A. Edwards, "Fuel Motion Measurements with In-Core Detectors," Technical Information Exchange Meeting on Fuel and Clad Motion Diagnostics in LMFBR Safety Test Facilities, Albuquerque, New Mexico (1975).

5. R. B. Shields, "A Platinum In-Core Flux Detector," IEEE Trans. Nucl. Sci., NS-20 (1973).

6. H. Boeck and M. Soleiman, "Development and Tests of a Self Powered Neutron Detector with a Fissile Emitter," International Symposium on Nuclear Power Plant Control and Instrumentation, Cannes, France, IAEA-SM-226/13, April 24-28, 1978.

7. J. H. Renken, Use of Solutions to the Adjoint Transport Equation for the Evaluation of Radiation Shield Designs, SC-RR-70-98, Sandia Laboratories, Albuquerque, New Mexico (1970).

8. G. E. Hansen and H. A. Sandmeier, "Neutron Penetration Factors Obtained by Using Adjoint Transport Calculations," Nucl. Sci. Eng., 22, 315 (1965).

9. G. I. Bell and S. Glasstone, Nuclear Reactor Theory (1970).

10. C. L. Lawson and R. J. Hanson, Solving Least Squares Problems (1974).

11. F. Biggs and D. E. Amos, Numerical Solutions of Integral Equations and Curve Fitting, SC-RR-71-0212, Sandia Laboratories, Albuquerque, New Mexico (1971).

CHAPTER 5

FLASH X-RADIOGRAPHY FOR MATERIAL MOTION DETECTION

L. M. Choate, W. H. Buckalew, and L. D. Posey
Sandia Laboratories, Albuquerque, New Mexico

The applicability of flash x-ray cinematography for the detection of material motion during reactor safety experiments is being studied at Sandia Laboratories. As part of this study, a comparison is being made between conventional radiographic and coded source radiographic techniques. For the conventional radiographic technique, the effects of photon buildup and photon scattering upon spatial and areal density resolution capabilities in poor geometry situations are being evaluated. Two particular methods of producing a coded radiographic source are under investigation.

The determination of the requisite x-ray source needed to satisfy experimental resolution requirements (spatial, temporal, and areal density) is of major importance. Consequently, the implications of the recently established DOE/NRC "concensus" experimental requirements for material motion detection upon system components (e.g., the bremsstrahlung source characteristics, active detection system performance capabilities etc.) are being evaluated.

A significant part of the experimental program dealing with the behavior of prototypic LMFBR fuel pin bundles under mild to severe power transients is that of the observation of fuel/cladding/coolant motion. The feasibility of using electron beam flash x-radiography as a diagnostic tool for safety test facilities (refer to the schematic representation of Figure 5.1) is presently under evaluation. A summary of the objectives and approach of the flash x-radiography program is presented in Figure 5.2.

Several areas of major importance are:

a. Spatial and Areal Density Resolution Capabilities

Experiments have been performed on a LINAC (5-10 MeV, < 1 mm diameter focal spot) to evaluate the effects of photon buildup upon spatial and areal density resolution capabilities in poor geometry situation. A schematic representation of the experiments is shown in Figure 5.3 (except that the stainless steel was removed). The source-to-object/object-to-image distances were 2.0 m/2.0 m with Type R x-ray film used as the detector.

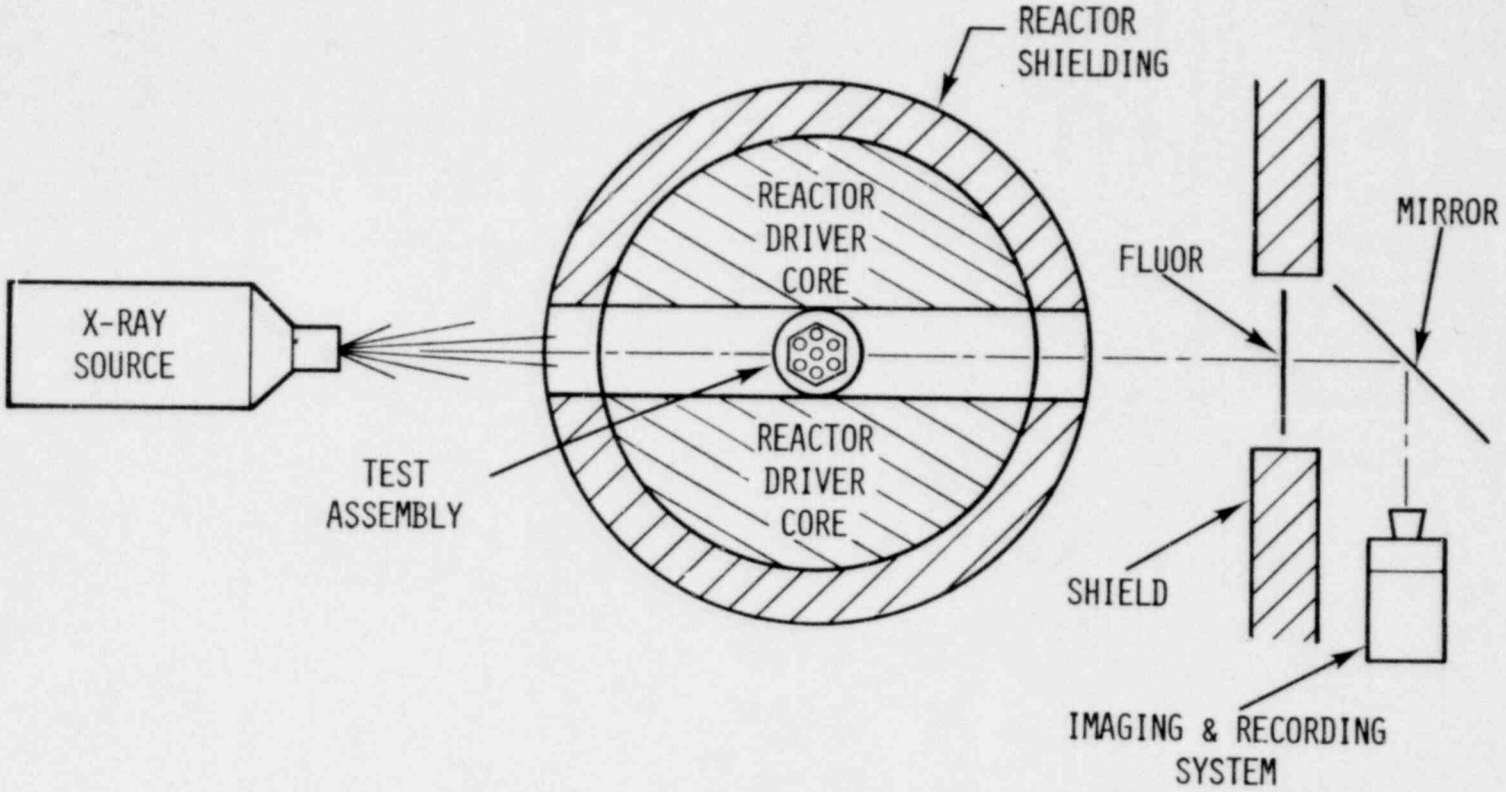

Figure 5.1. Electron Beam Flash X-Radiography for Fuel Motion Studies.

OBJECTIVES

Evaluate Feasibility of X-Ray Cinematography for Material Motion Detection

Evaluate Hardware and Associated Techniques for Use in a System of This Type

Determine Quantitative Performance Limitations of This Type of System

APPROACH

Evaluate Resolution Degradation Resulting from Photon Scattering and/or Buildup

Compare Conventional Radiography and Coded Source Radiography Techniques for High Intensity Applications

Evaluate Active Detector System Components

Based Upon Above Results Identify Required Bremsstrahlung Source Operating Characteristics

Figure 5.2. X-Ray Cinematography for Material Motion Detection.

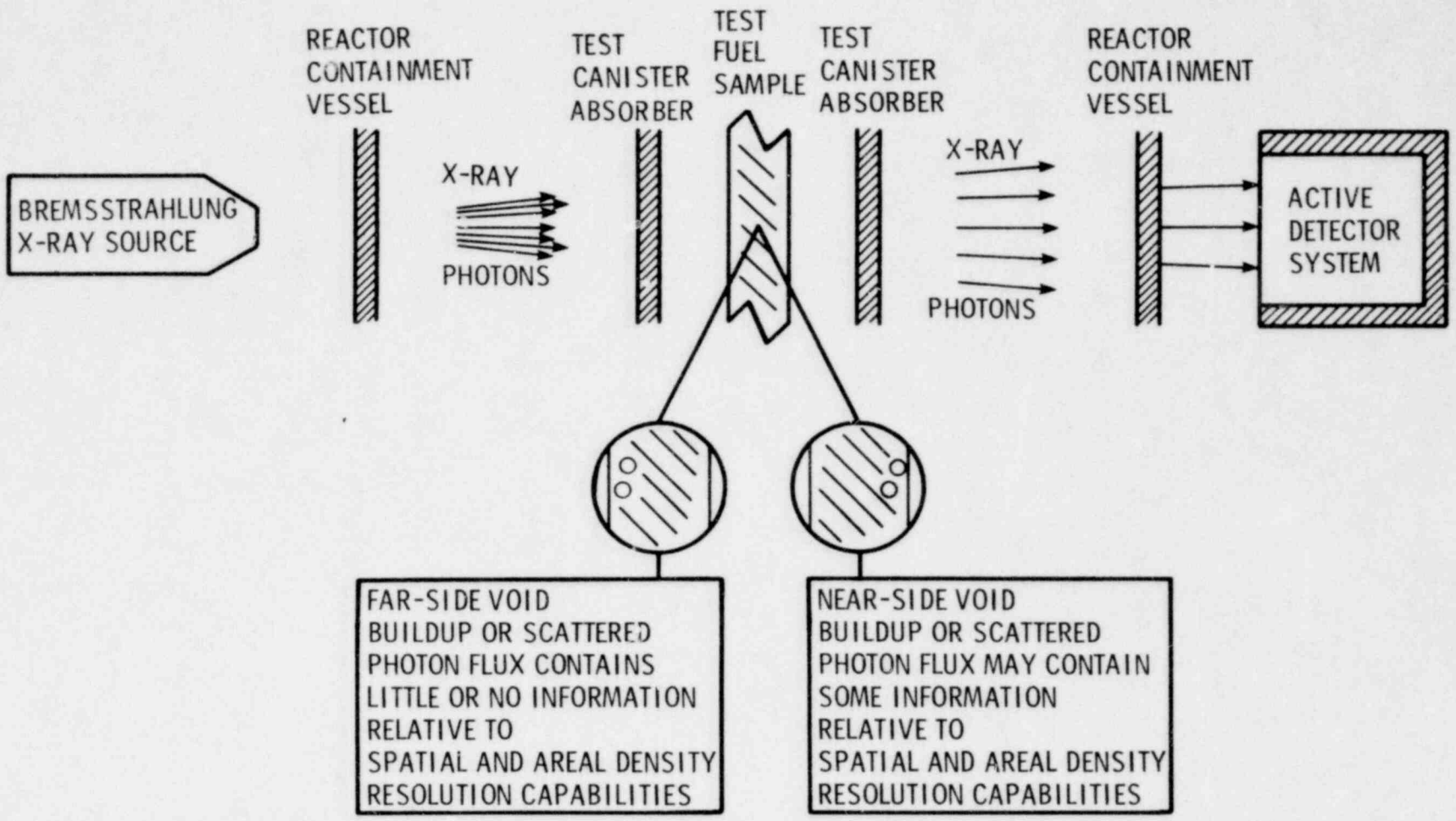

Figure 5.3. Resolution-Geometry Dependence (Void Size, Void Location, Endpoint Energy).

Figure 5.4 shows typical data in the form of optical density measurements for these experiments, while Figure 5.5 shows the overall results. In these measurements voids of varying geometry were introduced on the near- and far-side of a simulated 271 pin bundle. Resolution degradation was found to be more important at lower end point energies and for smaller voided regions. The degradation in areal density resolution was found to be more pronounced than for spatial resolution. These effects are found to be significantly mitigated at higher endpoint energies as well as by the presence of stainless steel which would comprise the containment structure walls for actual experimental situations. Work is continuing to evaluate the effects of scattered photons upon resolution capabilities. It is felt that resolution degradation should pose no significant problem for the requisite x-ray source although it could be important under severely distorted geometry situations.

b. Source Requirements and Performance Estimates

In light of the recently established DOE/NRC "concensus" experimental requirements for material motion detection it is now appropriate to further quantify source requirements and system performance based upon the best data available at present. For the purposes of further discussion a base-line source was defined with the following operating characteristics:

type - LINAC
energy - 30 MeV
current - 5 amp
pulse width - 1 μsec
pulsing rate - 1000 pps

These are quite similar to the operating characteristics of a machine proposed for this purpose by LASL. That source was estimated to cost in excess of 3 M$. Figure 5.6 shows the precision uncertainty (associated with a mass change of about 10%) obtainable with a machine of this energy and pulse width for a peak power of 10^5 W/g and resolution capabilities of type KK x-ray film and a hypothetical detector system which can perform 5 times better than KK film (both in terms of signal and background sensitivity). Using the machine specified above and these limits on detector system performance, the comparison of capabilities with requirements shown in Figure 5.7 was developed. As can be seen from these data, most of the range of operating conditions can be satisfied if precision uncertainties of 50 to

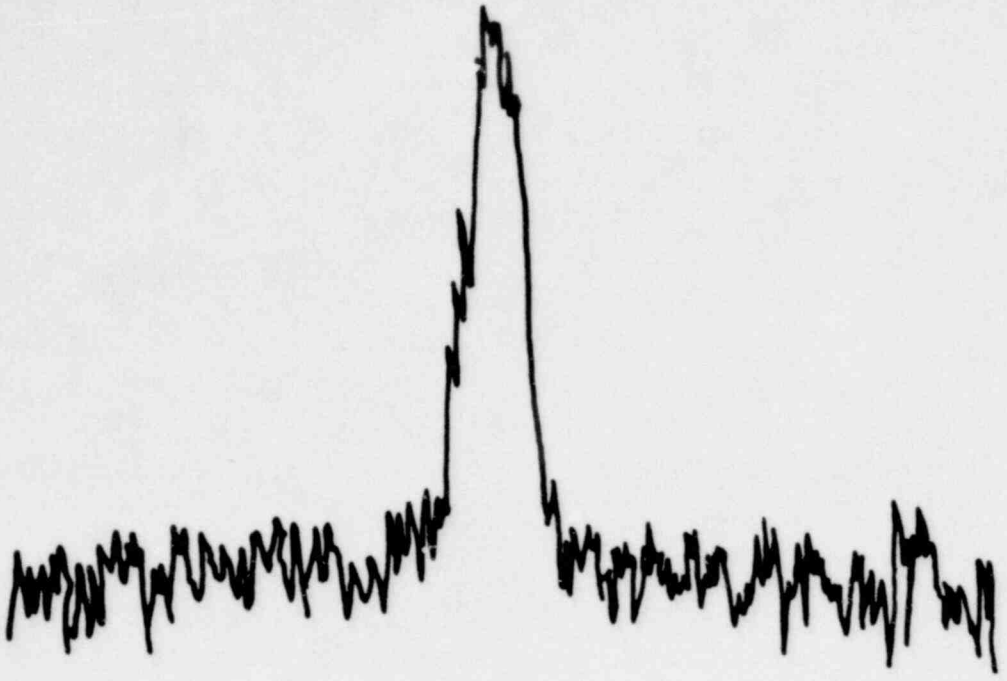

VOID ON NEAR-SIDE, 5 MeV LINAC ENERGY

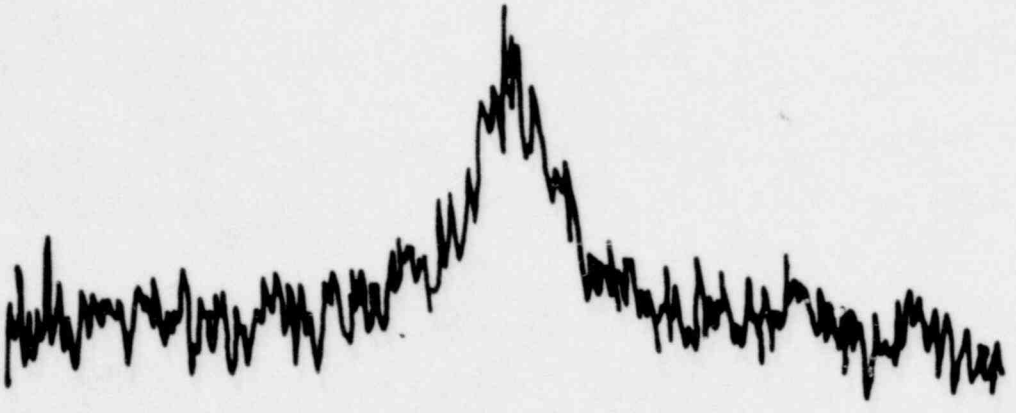

VOID ON FAR-SIDE, 5 MeV LINAC ENERGY

Figure 5.4. Areal Density Resolution Degradation from Photon Buildup Effects.

ENERGY (MeV)	5.0	7.5	10.0
NEAR-SIDE (gm/cm^2)	2.5	2.4	2.6
FAR-SIDE (gm/cm^2)	6.0	3.7	3.3
RATIO	0.40	0.65	0.80

(~ 14 gm/cm^2 VOID FORMED BY ~1 mm SLIT)

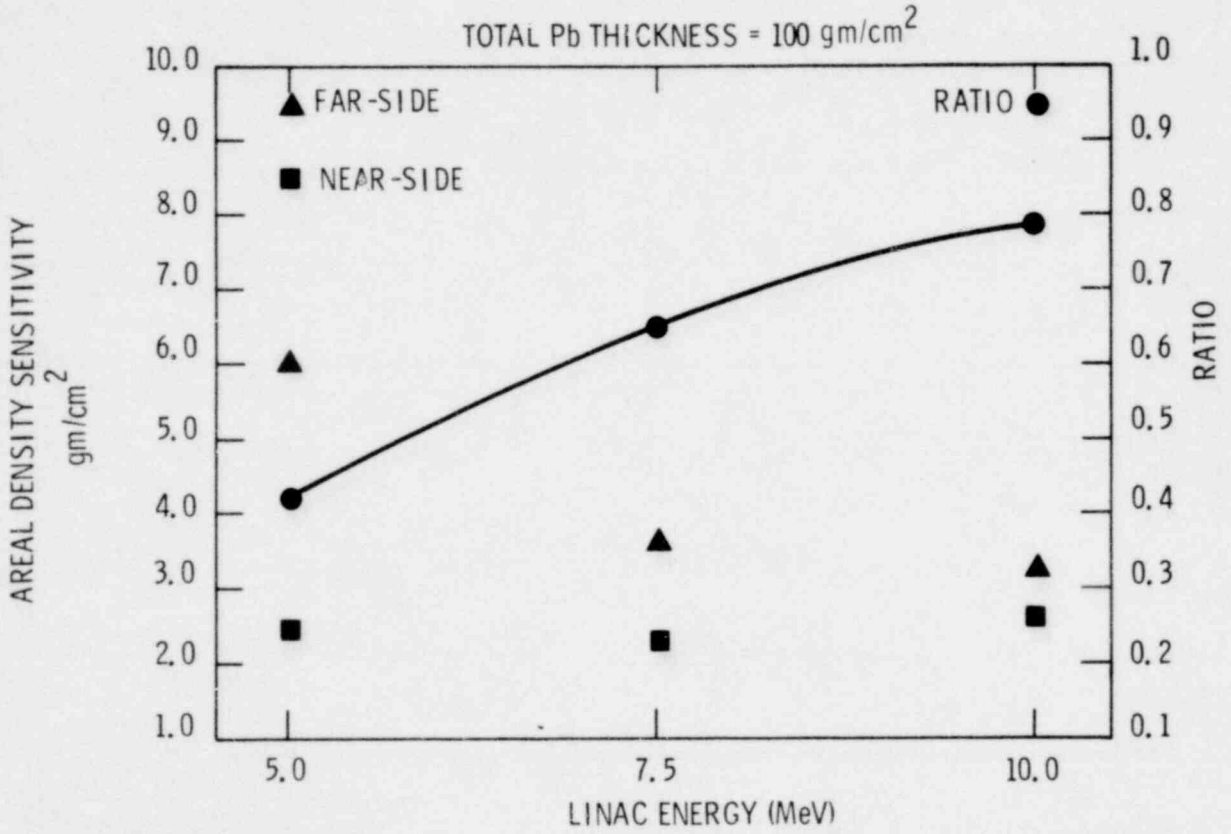

Figure 5.5. Threshold Areal Density Sensitivity (Various Endpoint Energy and Void Locations).

	TYPE KK X-RAY FILM	ACTIVE DETECTOR SYSTEM
PEAK POWER	10^5 W/G	
LINAC CHARACTERISTICS ENERGY CURRENT PULSE WIDTH	30 MeV 5 A 1 μ SEC	
BKG DOSE	0.1 RAD	0.02 RAD
PRECISION UNCERTAINTY ON APEX (76 GM/CM^2) ACROSS FLATS (41 GM/CM^2)	* $\pm$77%	$\pm$30% $\pm$14%

*Exceeds 100% and Therefore not Meaningful.

Figure 5.6. Precision Uncertainty Associated with 10 Percent Mass Change in 127 Pin Bundle Using Type KK X-Ray Film and a Hypothetical Active Detector System (5 Times as Sensitive as Film and 5 Times Less Sensitive to BKG). Note: System Nonlinearities not Considered in This Analysis.

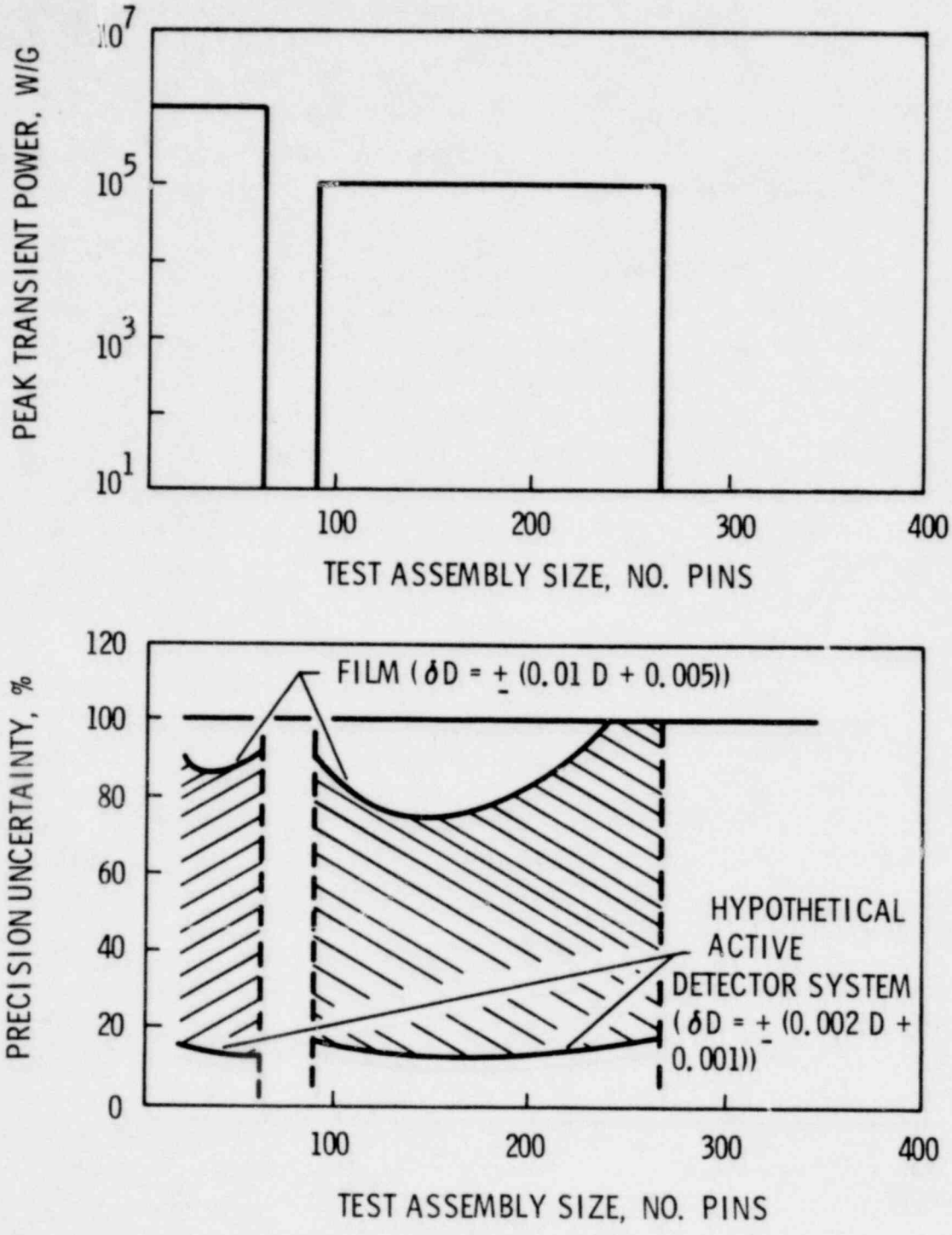

Figure 5.7. For Varying Test Assembly Size (# Pins) and Associated Peak Transient Power the Estimated Precision Uncertainty Range for a 10% Mass Change is Presented. The Source is the LINAC of Figure 5.6.

100% for a 10% mass change are acceptable. Should the performance goals for the active detector system postulated above not be realized then it would be necessary to increase the source current and/or energy in order to even achieve these rather modest mass change measurement capabilities. Therefore the possible need for a high intensity electron accelerator still exists and as a result, activity continues in the area of broad-area coded-beam generation. This work has potential application in DOE/OMA weapon effects experiments.

c. Conventional Radiography vs. Coded Source Radiography

For most applications conventional radiographic techniques should be able to satisfy most of the resolution requirements for smaller test bundles at most power densities. Extending present LINAC and LIA technology should yield the requisite source. However, for larger test bundles and high power densities, the coded source radiographic technique is necessary to achieve the required intensity levels. This technique would require a development effort in REB technology to achieve the necessary multiple pulsing capability. A comparison between the two radiographic techniques is presented in Figure 5.8.

d. Coded Source Technique vs. Coded Aperture Technique

Studies have been underway to evaluate the applicability of coded source radiography (electron modulation for producing desired coded x-ray beam) and coded aperture radiography (photon modulation for producing desired coded x-ray beam). Experiments have been performed on the HERMES-II accelerator (10 MeV endpoint energy, 130 kA, 50 ns FWHM, 50 k Rads(Si)/pulse) for both techniques.

Successful results have been obtained for the latter technique with pseudoholograms having been produced for a number of test objects ranging from one to several mock fuel pins. Both positive and negative apertures have been used with reconstructions of the test object images presently underway. Only moderately successful results have been obtained for the former case. Difficulty persists in eliminating unwanted background bremsstrahlung production and in finding a coded convertor design which survives successive pulses. A comparison of the source coding techniques is presented in Figure 5.9.

CONVENTIONAL RADIOGRAPHY

ADVANTAGES:

1. Established technology.
2. Machine source requirements satisfied by near state-of-the-art LINAC or LIA (some development may be necessary).
3. Good spatial, temporal, and areal density resolution capabilities; most resolution requirements can be satisfied.
4. Does not require unfolding of acquired data.
5. Pre- and post-test diagnostic capability.

DISADVANTAGES:

1. Intensity limited; small focal spot requirement limits available current.
2. No depth resolution.
3. Limits to bundle size and power densities for which data can be accumulated.
4. Requires a slot through reactor.
5. Difficult to distinguish between fuel, cladding, and coolant.

CODED SOURCE RADIOGRAPHY

ADVANTAGES:

1. Not intensity limited, broad beam allows high current.
2. Some depth resolution (dependent upon systems design).
3. Increased capability to bundle size and power densities for which data can be accumulated.
4. Pre- and post-test diagnostic capability.

DISADVANTAGES:

1. New technology.
2. Machine source requirements necessitate advances in REB technology (multiple pulsing requirements).
3. Poor to good spatial and areal density resolution capabilities.
4. Requires unfolding of acquired data.
5. Resolution capabilities may be limited to either internal fuel motion or to surface fuel motion.
6. Requires a slot through reactor.
7. Difficult to distinguish between fuel, cladding and coolant.

Figure 5.8. Electron Beam Flash X-Radiography Program for Material Motion Studies.

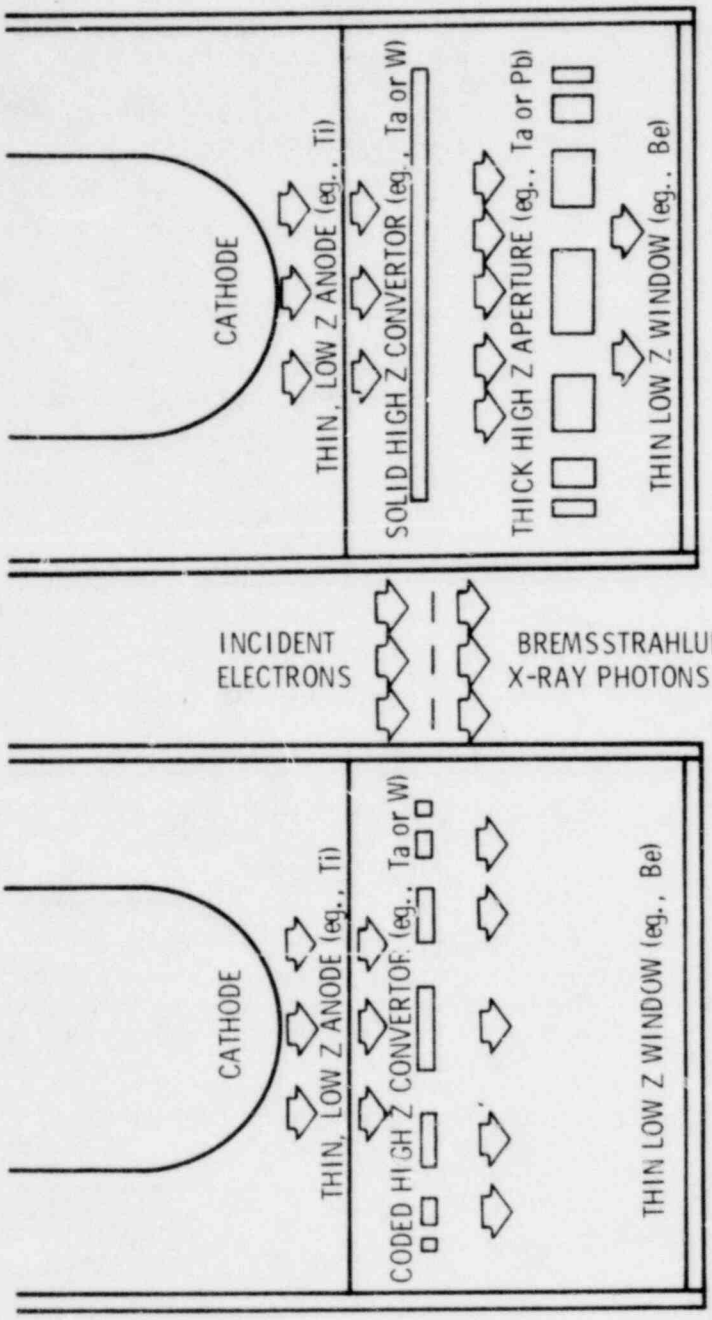

CODED APERTURE TECHNIQUE

(Negative Source Shown Here)

Method: Photon Modulation to Achieve Desired X-Ray Source
Modulation: Poor to Good
Field of View: Poor to Good
Advantages: Can achieve an optimum design for particular experimental requirements, easier technique
Disadvantages: Poor to good modulation and field of view depending upon experiment

CODED SOURCE TECHNIQUE

(Positive Source Shown Here)

Method: Electron Modulation to Achieve Desired X-Ray Source
Modulation: Good
Field of View: Good
Advantages: Good modulation and field of view
Disadvantages: Difficult to achieve an optimum design for particular experimental requirements, more difficult technique, unwanted background Bremsstrahlung production difficult to eliminate

Figure 5.9. Source Coding Techniques (Flash X-Ray Fuel Motion Program).

DISTRIBUTION:

US Nuclear Regulatory Commission
(310 copies for R7)
Division of Document Control
Distribution Services Branch
7920 Norfolk Avenue
Bethesda, MD 20014

US Nuclear Regulatory Commission (54)
Division of Reactor Safety Research
Office of Nuclear Regulatory Research
Washington, DC 20555
Attn: C. N. Kelber, Assistant Director,
Advanced Reactor Safety Research
R. T. Curtis, Chief
Analytical Advanced Reactor Safety Research, ARSR
M. Silberberg, Chief
Experimental Fast Reactor Safety
R. W. Wright (50)
Experimental Fast Reactor Safety

US Department of Energy
Office of Nuclear Safety Coordination
Washington, DC 20545
Attn: R. W. Barber

US Department of Energy (2)
Albuquerque Operations Office
P. O. Box 5400
Albuquerque, NM 87185
Attn: J. R. Roeder, Director
Operational Safety Division
D. K. Nowlin, Director
Special Programs Division
For: C. B. Quinn
D. Plymale

University of Michigan
Nuclear Engineering Department
Ann Arbor, MI 48104

General Electric Corporation
310 De Guigne Drive
Sunnyvale, CA 94086
Attn: J. O. Bradfute, Manager, Dynamics and Safety

W. E. Nyer
P. O. Box 1845
Idaho Falls, ID 83401

Projekt Schneller Brueter (4)
Kernforschungszentrum Karlsruhe GMBH
Postfach 3640
D75 Karlsruhe
West Germany
Attn: Dr. Kessler (2)
Dr. Heusener (2)

1437 180

Distribution (Cont'd)

Institut de Protection
et de Surete Nucleaire (3)
CEN Fontenay-aux-Roses
B. P. 6
92260 Fontenay-aux-Roses
France
Attn: M. Tanguy
M. Schmitt
M. Cogne

Safety Studies Laboratory (3)
Commissariat a L'Energie Atomique
Centre d'Etudes Nucleaires de Cadarache
B. P. 1, 1311S Saint-Paul-les-Durance
Bouches-Du-Rhone
France
Attn: M. Bailly
M. Meyer-Heine
M. Penet

Centre d'Etudes Nucleaires de Grenoble
B. P. 85, Centre de Tri
38401 Grenoble, Cedex
France
Attn: M. Costa

H. J. Teague (3)
UKAEA
Safety and Reliability Directorate
Wigshaw Lane
Culcheth
Warrington, WA3 4NE
England

R. G. Bellamy
Reactor Fuels Group
AERE Harwell
Oxfordshire, OX11 ORA
England

R. G. Tyror, Head
Reactor Development Division
UKAEA - Atomic Energy Establishment
Winfrith, Dorchester
Dorset
England

Power Reactor & Nuclear Fuel
Development Corporation (PNC) (2)
Fast Breeder Reactor Development Project (FBR)
9-13, 1-Chome, Akasaka
Minato-Ku, Tokyo
Japan
Attn: Dr. Mochizuki
Dr. Watanabe

Distribution (Cont'd)

1100 C. D. Broyles
Attn: G. E. Hansche, 1120
G. L. Ogle, 1125
H. E. Viney, 1130
J. H. Davis, 1136
1253 G. W. Gobeli
Attn: K. T. Stalker, 1253
1537 N. R. Keltner
Attn: R. U. Acton, 1537
T. Y. Chu, 1537
1550 F. W. Neilson
Attn: O. J. Burchett, 1552
J. H. Gieske, 1552
2150 T. L. Workman
3434 B. N. Yates
4000 A. Narath
4231 J. H. Renken
Attn: J. A. Halbleib, 4231
P. J. McDaniel, 4231
J. E. Morel, 4231
4400 A. W. Snyder
4410 D. J. McCloskey
4420 J. V. Walker
4422 R. L. Coats
4422 J. B. Rivard
4422 D. W. Varela
4423 J. E. Powell
4423 R. A. Beyerlein
4423 L. M. Choate
4423 J. G. Kelly
4423 D. A. McArthur
4423 H. L. Scott
4423 W. H. Sullivan
4423 S. A. Wright (5)
4424 P. S. Pickard
4424 J. T. Hitchcock
4424 D. R. Worledge
4425 W. J. Camp
4425 R. W. Ostensen
4425 D. C. Williams
4425 M. F. Young
4425 R. J. Lipinski
4425 W. M. Breitung
4425 Jean-Louis Portugal
4442 W. A. Von Riesemann
4450 J. A. Reuscher
4451 T. R. Schmidt
4452 L. D. Posey
4550 R. M. Jefferson
5500 O. E. Jones
Attn: O. E. Jones (Actg), 5510
D. F. McVey, 5511
D. O. Lee, 5511
R. D. Boyd, 5511
M. Corradini, 5511
H. C. Hardee, 5512
5530 W. Herrmann
Attn: D. A. Benson, 5534
J. E. Smaardyk, 5534

Distribution (Cont'd)

5800 R. S. Claassen
5820 R. E. Whan
5822 N. E. Brown
5830 M. J. Davis
Attn: R. W. Rohde, 5832
J. L. Ledman, 5833
5831 N. J. Magnani
5831 D. A. Powers
5835 C. H. Karnes
5846 R. A. Sallach
8266 E. A. Aas
3141 T. L. Werner (5)
3151 W. L. Garner (3)
For: DOE/TIC (Unlimited Release)
3154-3 R. P. Campbell (25)
For NRC Distribution to NTIS

1437 183

11

POOR ORIGINAL

Org.	Bldg.	Name	Rec'd by *	Org.	Bldg.	Name	Rec'd by *

* Recipient must initial on classified documents.

1437 184